

Matrix Factorization for Nonparametric Multi-Source Localization Exploiting Unimodal Properties

Junting Chen and Urbashi Mitra

Ming Hsieh Department of Electrical Engineering, University of Southern California
Los Angeles, CA 90089 USA, email: {juntingc, ubli}@usc.edu

Abstract—Herein, the problem of simultaneous localization of multiple sources given a number of energy samples at different locations is examined. The strategies do not require knowledge of the signal propagation models, nor do they exploit the spatial signatures of the source. A nonparametric source localization framework based on a matrix observation model is developed. It is shown that the source location can be estimated by localizing the peaks of a pair of location signature vectors extracted from the incomplete energy observation matrix. A robust peak localization algorithm is developed and shown to decrease the source localization mean squared error (MSE) faster than $\mathcal{O}(1/M^{1.5})$ with M samples. To extract the source signature vectors from a matrix with mixed energy from multiple sources, a unimodal-constrained matrix factorization (UMF) problem is formulated, and two rotation techniques are developed to solve the UMF efficiently. Our numerical experiments demonstrate that the proposed scheme achieves similar performance as the kernel regression baseline using only 1/5 energy measurement samples in detecting a single source, and the performance gain is more significant in the cases of detecting multiple sources.

Index Terms—Source localization, unimodal, sparse signal processing, matrix completion, nonparametric estimation

I. INTRODUCTION

Source localization is important in many domains, such as salvage, exploration, tactical surveillance, and hazard finding. However, in many application scenarios, it is difficult to obtain the correct propagation parameters of the source signal for localization. For example, in underwater localization with acoustic signals, the signal propagation depends on the water temperature, pressure, and salinity, which are location-dependent. In gas source localization, the gas diffusion characteristics depends on the chemical type and the atmospheric conditions. Therefore, model-based parametric localization methods [1]–[6] may not be reliable in application scenarios with a temporal and spatial varying nature.

Model-free positioning schemes, such as connectivity based localizations and weighted centroid localizations (WCL), have attracted a lot of interest due to their simplicity in implementation and the robustness to variations of propagation properties [7]–[12]. However, connectivity based techniques [7], [8] can only provide coarse localization results and the performance of WCL [9], [10] highly depends on the choice of parameters and the propagation environments. Recently, machine learning techniques, such as kernel regression and

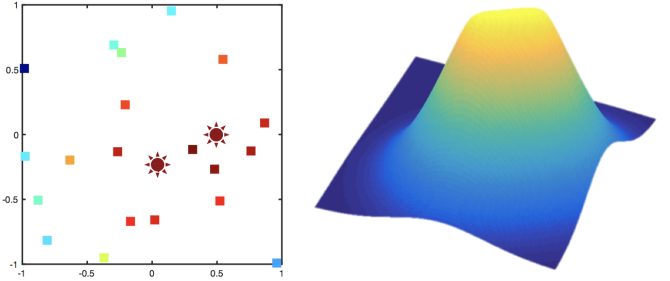


Figure 1. Left: Energy measurements at different locations (colored-squares) to localize two sources (red stars). Right: The underlying energy field appears as one peak when the two sources are close to each other.

support vector machines [13]–[15] have also been explored for localization. However, these methods usually require a separate training phase which may not be available in practice.

This paper studies nonparametric methods for localizing several sources based on a few energy measurements at different sensing locations as illustrated in Fig. 1. Our previous works studied the single source case in [11], [16], where a trust region was developed for targeting the source and a multi-step exploration-exploitation strategy was developed for active search using an underwater robot. The results were extended to the cases of two or more sources by exploiting novel coordinate system rotation techniques [12], [17]. However, these works were based on a decomposable assumption on the matrix formed by the energy measurements in a discretized 2D area.

In this paper, we find that the decomposable assumption is *not* necessary. Specifically, we show that the source location in 2D can be found by localizing the peaks of a pair of location *signature* vectors that are obtained from a sparsely observed energy matrix based on measurements in a discretized 2D area, and such a result holds *universally* as long as the signal energy decays in all directions away from the source location. Therefore, the method is robust in a lot of unknown propagation environments. In addition, we quantify the performance degradation when the actual energy matrix is not ideally rank-1. Based on this model, we develop strategies to localize multiple sources by overcoming three additional challenges: First, we formulate peak localization algorithms for noise corrupted vectors extracted from a sparse energy observation matrix. Second, we design matrix factorization techniques to extract the source signature vectors from the

This research has been funded in part by one or more of the following grants: ONR N00014-15-1-2550, NSF CNS-1213128, NSF CCF-1718560, NSF CCF-1410009, NSF CPS-1446901, and AFOSR FA9550-12-1-0215.

matrix that collects mixed energy from multiple sources. Note that the singular value decomposition (SVD) framework in our preliminary work [12], [16] does not work herein since the signature vectors may not be orthogonal. Third, we develop optimization techniques for the optimal rotation of the coordinate system, which determines how to arrange the measurements into the horizontal and vertical entries of the observation matrix.

To summarize, the following contributions are made herein:

- We propose an energy matrix observation model and prove that the matrix has a unimodal property, where the left and right dominant singular vectors, corresponding to each source, are unimodal with their peaks representing the source locations.
- We develop localization algorithms that exploit the unimodal and symmetric property. We prove that the location MSE decreases faster than $\mathcal{O}(1/M^{1.5})$ in the single source case.
- For the case of multiple sources, we develop optimization techniques to establish an optimal coordinate system with an rotation angle adaptive to the unknown source topology.
- We show that the optimal rotation can be found by maximizing the normalized dominant singular value of the observation matrix in the two source case.
- For the case of arbitrary number of sources, we solve a UMF problem and show that the convergence can be enhanced by rotating the coordinate system to minimize the normalized dominant singular value.

The rest of the paper is organized as follows. Section II establishes the matrix observation model and develops the unimodal property of source signature vectors. Section III studies the case of single source and develops the MSE localization performance. Section IV and V develop rotation optimization techniques for establishing the coordinate system in the two source and arbitrary number of sources cases. Numerical results are presented in Section VI and conclusion is given in Section VII.

Notation: Vectors are written as bold italic letters \mathbf{x} and matrices as bold capital italic letters \mathbf{X} . Random variables, random vectors, and random matrices are written as x , bold letters \mathbf{x} , and bold capital letters \mathbf{X} , respectively. For a matrix \mathbf{X} , X_{ij} denotes the entry in the i th row and j th column of \mathbf{X} . For a vector \mathbf{x} , x_i denotes the i th entry of \mathbf{x} . For a set \mathcal{X} , $|\mathcal{X}|$ denote the Cardinality of \mathcal{X} , i.e., the number of elements in \mathcal{X} . The notation $o(x)$ means $\lim_{x \rightarrow 0} o(x)/x \rightarrow 0$, and $\mathcal{O}(x)$ means $\limsup_{x \rightarrow 0} \mathcal{O}(x)/x < \infty$.

II. SYSTEM MODEL

A. Signal Model

Assume that there are K sources in an area with radius $L/4$. The location of source k is denoted by $\mathbf{s}_k \in \mathbb{R}^2$. The sources continuously emit signals that form an aggregated energy field, which can be measured at M different sensing locations that are distributed uniformly and randomly in the target area \mathcal{A} with radius $L/2$. Let $d(\mathbf{z}, \mathbf{s}) = \|\mathbf{z} - \mathbf{s}\|_2$ be the distance between the sensing location at $\mathbf{z} \in \mathbb{R}^2$ and a source location

\mathbf{s} . The energy measurement $\mathbf{h}^{(m)}$ at the m th sensing location $\mathbf{z}^{(m)}$ is given by

$$\mathbf{h}^{(m)} = \sum_{k=1}^K \alpha_k h(d(\mathbf{z}^{(m)}, \mathbf{s}_k)) + \mathbf{n}^{(m)} \quad (1)$$

where α_k is the transmit power of source k and $\mathbf{n}^{(m)}$ is the additive noise of the m th measurement with zero mean and variance σ_n^2 . The function $h(d)$ is a non-negative strictly decreasing function of the distance d from the source. In addition, we assume that $h(d)$ is Lipschitz continuous and square-integrable. Without loss of generality (w.l.o.g.), assume that $\iint_{\mathbb{R}^2} h(d(\mathbf{z}, \mathbf{s}))^2 d\mathbf{z} = 1$. Note that neither the source power α_k nor the function $h(d)$ are known.

B. Non-parametric Matrix Observation Model

1) *Matrix Model of the Energy Field:* We discretize the $L \times L$ area containing the target area, \mathcal{A} , into $N_1 \times N_2$ grid points. W.l.o.g., assume that $N_1 = N_2 = N \geq \sqrt{M}$, and the grid points are equally spaced.

Let $\mathbf{H}^{(k)} \in \mathbb{R}^{N \times N}$ be the discretized energy field matrix of source k , i.e., the (i, j) th element of $\mathbf{H}^{(k)}$ is given by

$$H_{ij}^{(k)} = \frac{L}{N} \alpha_k h(d(\mathbf{c}_{i,j}, \mathbf{s}_k)) \quad (2)$$

where $\mathbf{c}_{i,j} \in \mathbb{R}^2$ is the center location of the (i, j) th grid and the factor $\frac{L}{N}$ is for normalization purposes:

$$\begin{aligned} \|\mathbf{H}^{(k)}\|_F^2 &= \alpha_k^2 \sum_{i,j} \left(\frac{L}{N}\right)^2 h(d(\mathbf{c}_{i,j}, \mathbf{s}_k))^2 \\ &= \alpha_k^2 \iint_{\mathcal{A}} h(d(\mathbf{z}, \mathbf{s}_k))^2 d\mathbf{z} + o\left(\left(\frac{L}{N}\right)^2\right) \approx \alpha_k^2 \quad (3) \end{aligned}$$

where we have assumed that $h(d(\mathbf{z}, \mathbf{s}))$ has a negligible tail outside of \mathcal{A} , i.e., $\iint_{\mathbb{R}^2} h(d(\mathbf{z}, \mathbf{s}_k))^2 d\mathbf{z} \approx \iint_{\mathcal{A}} h(d(\mathbf{z}, \mathbf{s}_k))^2 d\mathbf{z}$.¹

Consider the SVD of $\mathbf{H}^{(k)} = \sum_i \sigma_{k,i} \mathbf{u}_{k,i} \mathbf{v}_{k,i}^T$, where $\sigma_{k,i}$ denote the i th largest singular value of $\mathbf{H}^{(k)}$. In particular, denote $\mathbf{u}_k = \mathbf{u}_{k,1}$ and $\mathbf{v}_k = \mathbf{v}_{k,1}$. Then, we have the following model for the K source energy field.

Definition 1 (Signature vector and signature matrix). The *signature matrix* for all K sources is defined as

$$\mathbf{H} \triangleq \sum_{k=1}^K \mathbf{H}^{(k)} = \sum_{k=1}^K \sigma_{k,1} \mathbf{u}_k \mathbf{v}_k^T + \sum_{k=1}^K \sum_{i=2}^N \sigma_{k,i} \mathbf{u}_{k,i} \mathbf{v}_{k,i}^T \quad (4)$$

where the vectors \mathbf{u}_k and \mathbf{v}_k , are called the *signature vectors* of source k .

Definition 2 (Unimodal). A vector $\mathbf{v} \in \mathbb{R}^N$ is unimodal if the following is satisfied:

$$0 \leq v_1 \leq v_2 \leq \dots \leq v_s \quad (5)$$

$$v_s \geq v_{s+1} \geq \dots \geq v_N \geq 0 \quad (6)$$

for some integer $1 \leq s \leq N$, where v_i is the i th entry of \mathbf{v} .

¹Note that the proposed algorithm does not require such an assumption. This approximation is just for the ease of discussion.

We show that the signature vectors \mathbf{u}_k and \mathbf{v}_k are unimodal and symmetric about the source location.

Theorem 1 (Unimodal Signature Vector). *The signature vectors \mathbf{u}_k and \mathbf{v}_k are unimodal. In addition, suppose that source k locates inside the (m, n) th grid. Then the peaks of \mathbf{u}_k and \mathbf{v}_k locate at the m th entry of \mathbf{u}_k and the n th entry of \mathbf{v}_k , respectively.*

Proof: See Appendix A. \square

Theorem 1 confirms the unimodal property of the signature vectors extracted from the rank one approximation of any energy field. Such a property holds universally as long as the propagated energy is a strictly decreasing function of the distance from the source. Note that the result in Theorem 1 is not trivial, as such a unimodal property does not hold for other singular vectors $\mathbf{u}_{k,i}$, $\mathbf{v}_{k,i}$, for $i = 2, 3, \dots, N$.

Consider a Cartesian coordinate system \mathcal{C} , where the x -axis corresponds to a row of the grid centers and the y -axis corresponds to a column. Denote the vector of x coordinates of a row $\mathbf{c}_{i,1}, \mathbf{c}_{i,2}, \dots, \mathbf{c}_{i,N}$ as $\mathbf{c}_X = [c_{X,1}, c_{X,2}, \dots, c_{X,N}]$ for all rows i , and the vector of y coordinates of a column $\mathbf{c}_{N,j}, \mathbf{c}_{N-1,j}, \dots, \mathbf{c}_{1,j}$ as $\mathbf{c}_Y = [c_{Y,1}, c_{Y,2}, \dots, c_{Y,N}]$ for all columns j .

Proposition 1 (Symmetric Signature Vector). *For each source k , the signature vectors can be approximated by unimodal and symmetric vectors $\hat{\mathbf{u}}_k$ and $\hat{\mathbf{v}}_k$, such that $|H_{ij}^{(k)} - \alpha_k \hat{u}_{k,i} \hat{v}_{k,j}| \leq \frac{K_h L}{\sqrt{2} N}$, where K_h is a bounded constant such that $|h(d_1) - h(d_2)| \leq K_h |d_1 - d_2|$ for all $d_1, d_2 \geq 0$. In addition, $\hat{\mathbf{u}}_k$ and $\hat{\mathbf{v}}_k$ can be obtained as $\hat{u}_{k,i} = \sqrt{L/N} w(c_{Y,i} + \delta_2 - s_{k,2})$ and $\hat{v}_{k,j} = \sqrt{L/N} w(c_{X,j} + \delta_1 - s_{k,1})$, where $[s_{k,1}, s_{k,2}] = \mathbf{s}_k$ are the source coordinates, $[\delta_1, \delta_2] = \mathbf{s}_k - \mathbf{c}_{m,n}$ is the distance from the source \mathbf{s}_k to the nearest grid center $\mathbf{c}_{m,n}$, and $w(x)$ is a non-negative, unimodal, and symmetric function, i.e., $w(x) \geq 0$, $w(x) = w(-x)$, and $\frac{d}{dx} w(x) < 0$ for $x > 0$.*

Proof: See Appendix B. \square

The results in Theorem 1 and Proposition 1 suggest a *decoupled* source localization strategy for the x coordinate and the y coordinate, respectively: the source location \mathbf{s}_k can be found from localizing the peaks of one-dimension data arrays \mathbf{u}_k and \mathbf{v}_k extracted as the dominant singular vectors of $\mathbf{H}^{(k)}$. Note that, by contrast, existing nonparametric methods (e.g., weighted centroid and kernel regressions) require iterative search in two-dimensional (or, in general, $2K$ -dimensional) source location space.

Such insight leads to the following observation model.

2) *Matrix Observation Model:* Let \mathbf{H} be the $N \times N$ observation matrix that contains the M energy measurements. Specifically, the (i, j) th entry of \mathbf{H} is given by

$$H_{ij} = \frac{L}{N} h^{(m)} \quad (7)$$

if the m th energy measurement is taken inside the (i, j) th grid. Note that the measurement location $\mathbf{z}^{(m)}$ may not be at the center $\mathbf{c}_{i,j}$ of the grid.

There are two strategies for constructing the observation matrix \mathbf{H} . In a *conservative construction*, we choose $N = \sqrt{M}$

and the matrix is fully observed.² We may extract the signature vectors directly from \mathbf{H} . In an *aggressive construction*, we choose $N > \sqrt{M}$ and the matrix \mathbf{H} is partially observed.

C. Problem Formulation

Denote by \mathcal{U}_s^N the cone specified by the unimodal constraints (5) – (6) for a fixed s . Denote $\mathcal{U}^N = \bigcup_{s=1}^N \mathcal{U}_s^N$ as the non-negative unimodal cone, and $\mathcal{U}^{N \times K}$ as the set of $N \times K$ real matrices where all the columns are in \mathcal{U}^N . Let $\mathbf{U}, \mathbf{V} \in \mathbb{R}^{N \times K}$ be the matrices that each contains K pairs of signature vectors $\{\mathbf{u}_k, \mathbf{v}_k\}$ to be determined. Let $\mathbf{W} \in \mathbb{R}^{N \times N}$ be an indicator matrix that describes the sampling strategy, where $W_{ij} = 1$, if $(i, j) \in \Omega$, and $W_{ij} = 0$, otherwise, where Ω denotes the set of entries that are assigned values based on (7), $|\Omega| = M$.

Based on the unimodal property developed in Theorem 1, we are interested in extracting from \mathbf{H} the vectors that are unimodal. Specifically, the source signature vectors can be extracted by solving the following *UMF* problem with missing values:

$$\mathcal{P}1: \underset{\mathbf{U}, \mathbf{V}}{\text{minimize}} \quad \|\mathbf{W} \odot (\mathbf{H} - \mathbf{U}\mathbf{V}^T)\|_F^2 \quad (8)$$

$$\text{subject to} \quad \mathbf{U} \in \mathcal{U}^{N \times K}, \mathbf{V} \in \mathcal{U}^{N \times K} \quad (9)$$

where \odot denotes the Hadamard product, i.e., $\mathbf{W} \odot \mathbf{H}$ is an $N \times N$ matrix computed entry-by-entry with $[\mathbf{W} \odot \mathbf{H}]_{ij} = W_{ij} H_{ij}$.

Note that the above sparse matrix factorization problem is formulated under a specific coordinate system \mathcal{C} . If we rotate the coordinate system θ degrees from a reference system \mathcal{C}_0 , the resulting rotated coordinate system is denoted by \mathcal{C}_θ . Then the problem $\mathcal{P}1$ is to find \mathbf{U}_θ and \mathbf{V}_θ from observation matrices \mathbf{H}_θ and \mathbf{W}_θ in the coordinate system \mathcal{C}_θ .

In general, $\mathcal{P}1$ is difficult to solve because the objective function is non-convex and the constraints are also non-convex. However, as to be discussed in the remaining part of this paper, there are some θ that make $\mathcal{P}1$ easier to solve. In the special cases of $K = 1, 2$, one can even find unique solutions to a relaxed version of $\mathcal{P}1$ for some coordinate system \mathcal{C}_θ .

III. SPECIAL CASE I: SINGLE SOURCE

In the single source case, the eigenstructure of the signature matrix \mathbf{H} is invariant under any rotation of the coordinate system \mathcal{C}_θ . We show that the factorization problem $\mathcal{P}1$ can be easily solved by a matrix completion problem followed by SVD. Therefore, the remaining challenge is to estimate the peaks of the signature vectors and to study the localization performance to justify the estimation strategy.

A. Solution via Matrix Completion

Without the unimodal constraints (9), $\mathcal{P}1$ is a classical rank- K matrix completion problem. It has been shown in the sparse signal processing literature that, under some mild

²For easy elaboration, assume that the M sensing locations distribute over M distinct grids.

regularization conditions on the low rank matrix \mathbf{H} (e.g., strong incoherence property and small rank property of \mathbf{H} , see [18], [19]), the matrix \mathbf{H} can be recovered, with a high probability, from the sparse and noisy observation $\mathbf{W} \odot \mathbf{H}$. Specifically, the noisy recovery of \mathbf{H} can be obtained as a solution, $\hat{\mathbf{X}}$, to the following convex optimization problem [16], [19]:

$$\begin{aligned} \mathcal{P}2: \quad & \underset{\mathbf{X}}{\text{minimize}} \quad \|\mathbf{X}\|_* \\ & \text{subject to} \quad \sum_{(i,j) \in \Omega} |X_{ij} - H_{ij}|^2 \leq \epsilon^2 \end{aligned} \quad (10)$$

where $\|\mathbf{X}\|_*$ denotes the nuclear norm of \mathbf{X} (i.e., the sum of the singular values of \mathbf{X}), and ϵ^2 is a small parameter (depending on the observation noise [19]) for the tolerance of the observation noise in \mathbf{H} .

Note that under exact recovery $\hat{\mathbf{X}} = \mathbf{H}$ in the $K = 1$ case, the signature vectors can be extracted from the SVD of the rank-1 matrix $\hat{\mathbf{X}} = \hat{\alpha}_1 \hat{\mathbf{u}}_1 \hat{\mathbf{v}}_1^T$. The unimodal constraints (9) are then automatically satisfied. As a result, an efficient solution to the sparse matrix factorization problem $\mathcal{P}1$ can be obtained as the dominant singular vectors of $\hat{\mathbf{X}}$ as the solution to $\mathcal{P}2$.

B. Peak Localization Exploiting Symmetry

We first establish the property of the symmetric function $w(x)$ specified in Proposition 1. The autocorrelation of $w(x)$ is given by

$$\tau(t) = \int_{-\infty}^{\infty} w(x)w(x-t)dx \quad (11)$$

which can be shown to be monotonic for $t > 0$.

Lemma 1 (Monotone property of $\tau(t)$). *The autocorrelation function $\tau(t)$ is non-negative and symmetric. In addition, $\tau(t)$ is strictly decreasing in $t > 0$.*

Proof: The result can be easily derived using the unimodal and symmetric property of $w(x)$. The details are omitted here due to page limit. \square

From Lemma 1, $\tau(t)$ is maximized as $t = 0$. As a result, the non-negative, unimodal, and symmetric function $w(x - s_{1,1})$ from Proposition 1 has the following autocorrelation function

$$\int_{-\infty}^{\infty} w(x - s_{1,1})w(-x + t - s_{1,1})dx \quad (12)$$

$$= \int_{-\infty}^{\infty} w(x - s_{1,1})w(x - t + s_{1,1})dx \quad (13)$$

$$= \int_{-\infty}^{\infty} w(z)w(z + 2s_{1,1} - t)dz \quad (14)$$

$$= \tau(t - 2s_{1,1})$$

which is maximized at $t = 2s_{1,1}$, where the first equality (13) is due to symmetry $w(x) = w(-x)$, and the second equality (14) is from the change of variable $z = x - s_{1,1}$.

Let $\hat{\mathbf{v}}_1$ be the dominant right singular of $\hat{\mathbf{X}}$, the solution to $\mathcal{P}2$. From Proposition 1, $\hat{\mathbf{v}}_1$ is a noisy discretization of $w(x - s_{1,1})$. As an estimate of the location $s_{1,1}$, the x coordinate of the source, can be given by

$$\hat{s}_{1,1}(\hat{\mathbf{v}}_1) = \frac{1}{2} \underset{t \in \mathbb{R}}{\text{argmax}} R(t; \hat{\mathbf{v}}_1) \quad (15)$$

where

$$R(t; \hat{\mathbf{v}}) = \int_{-\infty}^{\infty} \hat{v}(x)\hat{v}(-x+t)dx \quad (16)$$

is the *reflected correlation function* given $\hat{\mathbf{v}} \in \mathbb{R}^N$, in which, $\hat{v}(x)$ is a continuous (nonparametric) regression function based on $\hat{\mathbf{v}}$. For example, $\hat{v}(x)$ can be obtained by $v(x) = \hat{v}_i$ if $x = c_{X,i}$, $i = 1, 2, \dots, N$, and by linear interpolation between \hat{v}_i and \hat{v}_{i+1} if $c_{X,i} < x < c_{X,i+1}$, where \hat{v}_i is the i th entry of $\hat{\mathbf{v}}$.³

The estimator (15), as motivated by the form of the integral (12), computes the correlation of the data from both sides of the point the function $\hat{v}(x)$ is symmetric about. As a result, the peak location estimator from $\hat{\mathbf{v}}$ uses all N entries for estimation rather than merely a local subset of the entries around the peak location.

The location estimate, $\hat{s}_{1,2}$, from $\hat{\mathbf{u}}_1$ can be obtained in a similar fashion.

C. Squared Error Bound

Let $e(x) = \hat{v}(x) - w(x - s_{1,1})$ be the error between the non-parametric regression function $\hat{v}(x)$ obtained from interpolating $\hat{\mathbf{v}}_1$ and the function $w(x - s_{1,1})$ from Proposition 1. Define $\kappa = (\sigma_{1,1} - \sigma_{1,2})/\alpha_1$ as the normalized difference between the first dominant singular value and the second dominant singular value of the energy field matrix $\mathbf{H}^{(1)}$ in (4) for a single source. We have the following theorems to characterize the squared estimation error $\|\hat{\mathbf{s}}_1 - \mathbf{s}_1\|_2^2$ of the source location \mathbf{s}_1 .

We first consider the *conservative construction* of the observation matrix, where $N = \sqrt{M}$ and all the entries of \mathbf{H} are observed, and therefore the signature vectors $\hat{\mathbf{u}}_1$ and $\hat{\mathbf{v}}_1$ are directly extracted as the dominant left and right singular vectors of \mathbf{H} .

Theorem 2 (Squared Error Bound under the Conservative Construction). *Suppose that there exists $0 < C_e < \infty$, such that the interpolation error $e(x)$ satisfies $|\int_{-\infty}^{\infty} w(x - s_{1,1})[e(-x + t) - e(-x + t')]dx| \leq C_e |\int_{-\infty}^{\infty} w(x - s_{1,1})e(x)dx|$ for all $t, t' \geq 0$ and $N \rightarrow \infty$. Then, for $M = N^2$ under asymptotically large N ,*

$$\|\hat{\mathbf{s}}_1 - \mathbf{s}_1\|_2^2 \leq \frac{2C_e}{|\tau''(0)|\kappa^2} \left(\frac{4K_h^2 L^4}{N^3} + \frac{8L^2 \sigma_n^2}{N \alpha_1^2} \right) \quad (17)$$

with probability 1, where $\tau''(0)$ is the second order derivative of $\tau(t)$ evaluated at $t = 0$.

Proof: See Appendix C. \square

Remark 1. The terms K_h (Lipschitz continuity parameter) and $-\tau''(0)$ capture the sharpness of the energy field. For a Gaussian source energy field, $h(d) = \sqrt{2\gamma/\pi}e^{-\gamma d^2}$, one can calculate that $-\tau''(0) = \gamma$.

We now evaluate the case of the *aggressive construction*, where $N > \sqrt{M}$ and the matrix \mathbf{H} is partially observed. The

³Other nonparametric smoothing methods can be applied, such as k -nearest neighbor (KNN) regression and kernel regression [13], [14]. However, determining the best method to obtain $\hat{v}(x)$ is beyond the scope of this paper.

signature vectors $\hat{\mathbf{u}}_1$ and $\hat{\mathbf{v}}_1$ are extracted from $\hat{\mathbf{X}}$, a solution to the matrix completion problem $\mathcal{P}2$ based on \mathbf{H} .

Theorem 3 (Squared Error Bound under the Aggressive Construction). *Suppose that the measurement noise $n^{(m)}$ is bounded by $|n^{(m)}| < \bar{\sigma}_n$ and the sampling error of \mathbf{H} is bounded as $\sum_{(i,j)} |H_{ij} - \hat{H}_{ij}|^2 \leq \epsilon^2$, where ϵ is the parameter used in $\mathcal{P}2$. Assume that the matrix dimension $N = N(M)$ is chosen as the largest integer such that $M \geq \beta CN(\log N)^2$ for some constant C and β . Then, under the condition of Theorem 2, for asymptotically large N ,*

$$\|\hat{\mathbf{s}}_1 - \mathbf{s}_1\|_2^2 \leq \frac{512C_e L^2}{|\tau''(0)|\kappa^2} \left(\frac{K_h^2 L^2}{2N^2} + \frac{\sqrt{2}K_h L \bar{\sigma}_n}{N \alpha_1} + \frac{\bar{\sigma}_n^2}{\alpha_1^2} \right) \quad (18)$$

with high probability.

Proof: See Appendix C. \square

We draw the following observations from the analytical results in Theorems 2 and 3.

Efficiency of the Signature Matrix Model \mathbf{H} : The parameter $0 < \kappa \leq 1$ captures how precisely the outer product $\mathbf{u}_1 \mathbf{v}_1^T$ of the signature vectors may approximate the energy field matrix \mathbf{H} for a single source. In the ideal case where \mathbf{H} is rank-1, we have $\kappa = 1$ leading to a low MSE. For most practical propagation models we have tested (*e.g.*, propagations of radio signals over the air, acoustic signals in the water, etc.), κ is close to 1.

Performance Advantage of the Aggressive Construction Strategy: It can be verified that in the high signal-to-noise ratio (SNR) case $\alpha_1/\sigma_n^2, \alpha_1/\bar{\sigma}_n^2 \gg 1$, as the number of samples M increases, the squared error bound (18), which exploits matrix completion techniques under partial sampling, decreases at a higher rate in terms of M than the result in (17) under full sampling. Therefore, with a proper choice of the parameters β and C , the aggressive construction strategy can achieve the same localization performance using fewer measurements.

Sparsity and Noise Suppression Tradeoff: While the aggressive construction strategy achieves higher squared error decay rate in terms of the number of samples M under high SNR $\triangleq \alpha_1/\sigma_n^2 \gg 1$, it is less tolerant of measurement noise as observed from the last terms in (17) and (18), respectively. Specifically, in the low SNR case, the squared error bound of the aggressive construction strategy scales as $\mathcal{O}(\frac{1}{\text{SNR}})$, whereas, it scales as $\mathcal{O}(\frac{1}{N\text{SNR}})$ for the conservative construction strategy.

Performance Scaling Law: As a performance benchmark, for a naive scheme that estimates the source location directly from the position of the measurement sample that observes the highest power, the localization squared error decreases as $\mathcal{O}(1/M)$, whereas, even for the conservative construction case $N = \sqrt{M}$ of the proposed scheme, the squared error decreases as $\mathcal{O}(1/M^{3/2})$ in high SNR case $\alpha_1/\sigma_n^2 \gg 1$, order-wise faster than the naive scheme. These results then confirm that by exploiting the unimodal and symmetry properties as well as sparse signal processing techniques, the proposed algorithm will significantly improve the localization resolution.

IV. SPECIAL CASE II: TWO SOURCES

In the case of two sources, the SVD may not extract the desired signature vectors from \mathbf{H} in (4), because \mathbf{u}_1 and \mathbf{u}_2 are not necessarily orthogonal. However, it turns out that by choosing an appropriate coordinate system \mathcal{C} , the UMF problem $\mathcal{P}1$ can be trivially solved (under some mild conditions). In this section, we propose rotation techniques to select the optimal coordinate system for source separation and localization.

A. Optimal Rotation of the Coordinate System

We fix the origin at the center of the target area and rotate the coordinate system such that the two sources are aligned, w.l.o.g., on the y axis. Thus, the source locations satisfy $s_{1,1} = s_{2,1}$. Correspondingly, the signature vectors $\mathbf{v}_1 = \mathbf{v}_2$, since they are discretized from $w(x - s_{1,1})$ according to Proposition 1. This approximately yields a rank-1 model $\mathbf{H} = (\alpha_1 \mathbf{u}_1 + \alpha_2 \mathbf{u}_2) \mathbf{v}_1^T$ by ignoring the minor components in (4).

As a result, an algorithm for the two source case can be designed as follows. First, extract the vectors $\hat{\alpha}_1 \hat{\mathbf{u}}_1 + \hat{\alpha}_2 \hat{\mathbf{u}}_2$ and $\hat{\mathbf{v}}_1$ by solving the matrix completion problem $\mathcal{P}2$ followed by the SVD as developed in Section III. Second, obtain $\hat{\mathbf{u}}_1$ and $\hat{\mathbf{u}}_2$ from the composite vector $\hat{\alpha}_1 \hat{\mathbf{u}}_1 + \hat{\alpha}_2 \hat{\mathbf{u}}_2$. If the signature vectors in (4) are unimodal, then the solutions obtained will also satisfy the unimodal constraint (9).

The remaining challenge is to find the optimal rotation based on the M measurement samples as the source topology is not known.

Denote $\mathbf{H}(\theta)$ as the observation matrix constructed in coordinate system \mathcal{C}_θ with θ degrees of rotation to reference coordinate system \mathcal{C} . The desired rotation θ can be obtained as

$$\mathcal{P}3: \quad \underset{\theta \in [0, \frac{\pi}{2}]}{\text{maximize}} \quad \rho(\theta) \triangleq \frac{\sigma_1^2(\mathbf{H}(\theta))}{\sum_{k=1}^N \sigma_k^2(\mathbf{H}(\theta))} \quad (19)$$

where $\sigma_k(\mathbf{H})$ is defined as the k th largest singular value of $\hat{\mathbf{X}}(\mathbf{H})$, the solution to the matrix completion problem $\mathcal{P}2$ based on \mathbf{H} .

Note that $\rho(\theta) \leq 1$ for all $\theta \in [0, \frac{\pi}{2}]$. In addition, $\rho(\theta^*) = 1$, when $\mathbf{H}(\theta)$ becomes a rank-1 matrix where the sources are aligned with one of the axes.

The optimization problem $\mathcal{P}3$ is, in general, non-convex. An exhaustive search for the solution θ^* is computationally expensive, since for each θ , problem $\mathcal{P}2$ might need be solved followed by the SVD to obtain the singular value profile of $\mathbf{H}(\theta)$. However, it can be shown that $\rho(\theta)$ has a nice property that enables efficient optimization.

Let $\mathbf{H}(\theta)$ be the signature matrix defined in (4) under the coordinate system \mathcal{C}_θ . If $\mathbf{H}(\theta)$ can be perfectly recovered from $\mathbf{H}(\theta)$, *i.e.*, $\hat{\mathbf{X}}(\mathbf{H}(\theta)) = \mathbf{H}(\theta)$, we can show a locally unimodal property of $\rho(\theta)$.

Theorem 4 (Property of $\rho(\theta)$). *Assume that the two sources have equal transmission power $\alpha_1 = \alpha_2$. In addition, suppose that $\lambda_k(\mathbf{H}(\theta)) = \lambda_k(\mathbf{H}(\theta))$ for $k = 1, 2$. Then, $\rho(\theta)$ is periodic, *i.e.*, $\rho(\theta) = \rho(\theta + \frac{\pi}{2})$. In addition, $\rho(\theta)$ is strictly increasing over $(\theta^* - \frac{\pi}{4}, \theta^*)$ and strictly decreasing over*

$(\theta^*, \theta^* + \frac{\pi}{4})$, if the energy field satisfies

$$s \cdot \tau'(t) > t \cdot \tau'(s) \quad (20)$$

for all $0 < s < t$, where $\tau'(t) \triangleq \frac{d}{dt}\tau(t)$ and θ^* is the maximizer of $\rho(\theta)$.

Proof: See Appendix D. \square

The result in Theorem 4 confirms that the function $\rho(\theta)$ has a unique local maximum within a $\frac{\pi}{2}$ -window under a mild condition, in the ideal case of perfect recovery $\hat{\mathbf{X}}(\mathbf{H}(\theta)) = \mathbf{H}(\theta)$. The property motivates a simple bisection search algorithm to efficiently search for the globally optimal solution, θ^* , to (19).

Note that condition (20) can be satisfied by a variety of energy fields. For example, for Laplacian field $h(x, y) = \gamma e^{-\gamma|x| - \gamma|y|}$, we have the autocorrelation function $\tau(t) = (1 + \gamma t)e^{-\gamma t}$, and its derivative $\tau'(t) = -\gamma^2 t e^{-\gamma t}$; for Gaussian field $h(d) = \sqrt{2\gamma/\pi} e^{-\gamma d^2}$, where $d^2 = x^2 + y^2$, we have $\tau(t) = e^{-\gamma t^2/2}$, and $\tau'(t) = -\gamma t e^{-\gamma t^2/2}$. In both cases, condition (20) is satisfied.

B. Source Separation

Suppose that in the coordinate system \mathcal{C}_θ , the sources are aligned with the y axis. Then, the dominant left and right singular vectors of $\mathbf{H}(\theta)$ are proportional to $\alpha_1 \mathbf{u}_1 + \alpha_2 \mathbf{u}_2$ and \mathbf{v}_1 , respectively. Denote the dominant left and right singular vectors of $\hat{\mathbf{X}}(\mathbf{H}(\theta))$ (solution to $\mathcal{P}2$) as $\hat{\mathbf{u}}_1$ and $\hat{\mathbf{v}}_1$, respectively. Using a technique similar to that in Section III, we can estimate the x coordinate from

$$\hat{s}_{1,1} = \hat{s}_{2,1} = \frac{1}{2} \operatorname{argmax}_{t \in \mathbb{R}} R(t; \hat{\mathbf{v}}_1). \quad (21)$$

To find the y coordinates, if the two sources have equal transmission power $\alpha_1 = \alpha_2$, the combined signature vector $\alpha_1 \mathbf{u}_1 + \alpha_2 \mathbf{u}_2$ is symmetric about the mid-point $c = (s_{1,2} + s_{2,2})/2$, which can be estimated as

$$\hat{c} = \frac{1}{2} \operatorname{argmax}_{t \in \mathbb{R}} R(t; \hat{\mathbf{u}}_1). \quad (22)$$

As the two sources have equal distance r to the mid-point $(s_{1,1}, c)$, the variable r can be estimated as

$$\hat{r} = \operatorname{argmax}_{r \geq 0} Q(r; \hat{\mathbf{u}}_1, \hat{\mathbf{v}}_1) \quad (23)$$

where

$$Q(r; \hat{\mathbf{u}}_1, \hat{\mathbf{v}}_1) \triangleq \frac{1}{2} \int_{-\infty}^{\infty} \hat{u}(x) (\hat{v}(x - \hat{c} - r) + \hat{v}(x - \hat{c} + r)) dx$$

in which, $\hat{u}(x)$ is a non-parametric regression function from the interpolation of $\hat{\mathbf{u}}_1$ and $\hat{v}(x)$ is from interpolating $\hat{\mathbf{v}}_1$. Using calculations similar to (12) – (14), it can be shown that $Q(r; \mathbf{u}_1 + \mathbf{u}_2, \mathbf{v}_1)$ is maximized at $r^* = (s_{1,2} - s_{2,2})/2$ if the interpolation is perfect, i.e., $\hat{u}(x) = w(x - s_{1,2}) + w(x - s_{2,2})$ and $\hat{v}(x - s_{1,1}) = w(x - s_{1,1})$.

As a result, the estimated source locations are given by $\hat{\mathbf{s}}_1 = (\hat{s}_{1,1}, \hat{c} + \hat{r})$ and $\hat{\mathbf{s}}_2 = (\hat{s}_{2,1}, \hat{c} - \hat{r})$.

As a benchmark, consider a naive scheme that estimates $s_{1,2}$ and $s_{2,2}$ by finding the peaks of $\hat{\mathbf{u}}_1$. However, such a naive strategy cannot work for close spread sources, because the effective energy field function $\alpha_1 h(d(\mathbf{z}, \mathbf{s}_1)) + \alpha_2 h(d(\mathbf{z}, \mathbf{s}_2))$

that is observed would be unimodal with only one peak in $\hat{\mathbf{u}}_1$. As a comparison, the proposed procedure (21) – (23) can resolve such a limitation.

V. ARBITRARY NUMBER OF SOURCES

In the case of an arbitrary number of sources, we first study a general algorithm framework to solve $\mathcal{P}1$. We then discuss efficient approximations for fast implementation of the algorithm. Finally, an optimization of the coordinate system \mathcal{C}_θ is studied to enhance the convergence of the algorithm.

A. The Gradient Projection

Let $f(\mathbf{U}, \mathbf{V}) = \|\mathbf{W} \odot (\mathbf{H} - \mathbf{U}\mathbf{V}^T)\|_F^2$. With some algebra and matrix calculus, it can be shown that the gradients of f are

$$\frac{\partial}{\partial \mathbf{U}} f = -2(\mathbf{W} \odot \mathbf{H})\mathbf{V} + 2(\mathbf{W} \odot (\mathbf{U}\mathbf{V}^T))\mathbf{V}$$

$$\frac{\partial}{\partial \mathbf{V}} f = -2(\mathbf{W}^T \odot \mathbf{H}^T)\mathbf{U} + 2(\mathbf{W}^T \odot (\mathbf{V}\mathbf{U}^T))\mathbf{U}$$

and the iteration of the projected gradient algorithm can be computed as

$$\mathbf{U}(t+1) = \mathcal{P}_U \left\{ \mathbf{U}(t) - \mu_t \frac{\partial}{\partial \mathbf{U}} f(\mathbf{U}(t), \mathbf{V}(t)) \right\} \quad (24)$$

$$\mathbf{V}(t+1) = \mathcal{P}_V \left\{ \mathbf{V}(t) - \nu_t \frac{\partial}{\partial \mathbf{V}} f(\mathbf{U}(t+1), \mathbf{V}(t)) \right\} \quad (25)$$

where $\mathcal{P}_U\{\cdot\}$ is a projection operator to project any $N \times K$ matrix onto the unimodal cone $\mathcal{U}^{N \times K}$, and the step size μ_t and ν_t are chosen to ensure the decrease of the objective function f (for example, using a back-pressure rule).

B. Efficient Unimodal Projection

The projection $\mathcal{P}_U\{\mathbf{X}\}$ onto the unimodal cone is formally defined as the solution that minimizes $\|\mathbf{X} - \mathbf{Y}\|_F$ over $\mathbf{Y} \in \mathcal{U}^{N \times K}$. Due to the property of the Frobenius norm, the projection can be computed column-by-column.

While it is not straight-forward to efficiently project onto the convex set \mathcal{U}_s^N (specified by constraints (5) – (6)) as it may seem to be, it is relatively easier to compute the projection onto an *isotonic cone*, where an isotonic sequence is defined as a non-increasing (or non-decreasing) sequence. Recently, a fast algorithm for exact isotonic projection was developed in [20], which finds the solution within $N - 1$ steps.

With such a tool, a fast approximate algorithm to compute $\mathcal{P}_U\{\mathbf{X}\}$ can be described as follows.

Fast approximate unimodal projection:

- 1) For each s , compute the isotonic projection for \mathbf{x}_k , the k th column of \mathbf{X} , to form an ascending branch $y_1, y_2, \dots, y_s^{(1)}$ and a descending branch $y_s^{(2)}, y_{s+1}, \dots, y_N$, respectively, using the exact isotonic projection algorithm in [20].
- 2) Let $y_s = \max\{y_s^{(1)}, y_s^{(2)}\}$. Then, $\tilde{\mathbf{x}}_k^{(s)} := (y_1, y_2, \dots, y_s, \dots, y_N)$ is an approximate unimodal projection for \mathbf{x}_k with the k th entry taking the maximum value.

Table I
EVALUATION OF UNIMODAL PROJECTION ALGORITHMS, $\epsilon^2 = 10^{-10}$

Vector Size	Brute-force	Proposed	$\mathbb{E}\{e^2\}$	$\mathbb{P}\{e > \epsilon\}$
$N = 10$	2.28 sec	6.41 ms	1.5×10^{-3}	0.078
$N = 20$	5.13 sec	20.5 ms	1.8×10^{-10}	0.053

- 3) Repeat the previous steps to compute a series of projections for $s = 1, 2, \dots, N$.
- 4) Choose the solution $\tilde{\mathbf{x}}_k^{(s)}$ that minimizes $\|\tilde{\mathbf{x}}_k^{(s)} - \mathbf{x}_k\|$ over $s = 1, 2, \dots, N$.

where Step 2) is an approximation because the way in which y_s is determined is not optimal.⁴ Since Step 1) has complexity at most N , the overall complexity is at most N^2 .

In Table I, we compare the performance of the proposed fast projection with a brute-force projection method over independent and identically distributed (i.i.d.) standard Gaussian vectors $\mathbf{x} \sim \mathcal{N}(\mathbf{0}, \mathbf{I}_{N \times N})$. In the brute-force method, the vector \mathbf{x} is projected to the unimodal cone by solving N convex problems: $\tilde{\mathbf{x}}^{(s)} = \arg \min \|\mathbf{y} - \mathbf{x}\|_2$ subject to (5) – (6), for $s = 1, 2, \dots, N$, and pick $\tilde{\mathbf{x}}^* = \tilde{\mathbf{x}}^{(s)}$ to minimize $\|\tilde{\mathbf{x}}^{(s)} - \mathbf{x}\|_2$. The projection error is defined as $e = \|\tilde{\mathbf{x}} - \tilde{\mathbf{x}}^*\|_2 / \|\tilde{\mathbf{x}}^*\|_2$, where $\tilde{\mathbf{x}}$ is the solution of the proposed method. It is shown that the proposed fast approximate projection is more than 200 times faster, but has only marginal performance loss.

C. Local Convergence Analysis

Specifically, we frame the analysis according to the following two points. First, it is observed that the globally optimal solution $\hat{\mathbf{X}} = (\hat{\mathbf{U}}, \hat{\mathbf{V}})$ is in the interior of the unimodal cone $\mathcal{U}^{N \times K} \times \mathcal{U}^{N \times K}$, i.e., the unimodal constraints are not active when the algorithm iterate approaches the neighborhood of $\hat{\mathbf{X}}$. As a result, problem (8) becomes an unconstrained one in the neighborhood of $\hat{\mathbf{X}}$.

Second, note that the function is bi-convex. Therefore, we can study partial convergence, where the convergence of the variable \mathbf{U} is analyzed while fixing the other variable \mathbf{V} to be in the neighborhood of $\hat{\mathbf{V}}$. Thus, such analysis serves as a qualitative prediction on the convergence performance.

Denote $g(\mathbf{X}) = [(\partial f / \partial \mathbf{U})^T (\partial f / \partial \mathbf{V})^T]^T$ as the gradient function of $f(\mathbf{X})$, where $\mathbf{X} = (\mathbf{U}, \mathbf{V})$. Suppose $\mathbf{X}(0)$ is sufficiently close to $\hat{\mathbf{X}}$, such that the unimodal constraints are not active. As a continuous counter-part to the discrete iteration (24) – (25), the continuous algorithm trajectory $\mathbf{X}(t)$ can be given as

$$\frac{d}{dt} \mathbf{X}(t) = -g(\mathbf{X}(t)). \quad (26)$$

Let $\mathcal{E}(\mathbf{X}_e(t)) = \frac{1}{2} \|\mathbf{X}_e(t)\|_F^2$ be the normed error function for the convergence error $\mathbf{X}_e(t) \triangleq \mathbf{X}(t) - \hat{\mathbf{X}}$. Let $\mathbf{U}_e = \mathbf{U} - \hat{\mathbf{U}}$ and $\mathbf{V}_e = \mathbf{V} - \hat{\mathbf{V}}$ with the time index t dropped for notational brevity. The following result suggests that if either \mathbf{U}_e or \mathbf{V}_e is much smaller than the other variable, then the algorithm trajectory $\mathbf{X}(t)$ converges exponentially to $\hat{\mathbf{X}}$.

Proposition 2 (Partial convergence). *Assume perfect sampling $\mathbf{H} = \mathbf{H}$ and \mathbf{H} in (4) has rank K . Suppose that the algorithm initialization $\mathbf{X}(0)$ is close enough to the optimal solution $\hat{\mathbf{X}}$ to $\mathcal{P}1$. Then the following holds*

$$\frac{d}{dt} \mathcal{E}(\mathbf{X}_e) \leq -2\lambda_K(\hat{\mathbf{V}}^T \hat{\mathbf{V}}) \|\mathbf{U}_e\|_F^2 + o(\|\mathbf{U}_e\|_F^2) \quad (27)$$

for $\|\mathbf{V}_e\|_F = o(\|\mathbf{U}_e\|_F)$, where $\lambda_K(\mathbf{A})$ denotes the smallest eigenvalue of \mathbf{A} . Moreover,

$$\frac{d}{dt} \mathcal{E}(\mathbf{X}_e) \leq -2\lambda_K(\hat{\mathbf{U}}^T \hat{\mathbf{U}}) \|\mathbf{V}_e\|_F^2 + o(\|\mathbf{V}_e\|_F^2) \quad (28)$$

for $\|\mathbf{U}_e\|_F = o(\|\mathbf{V}_e\|_F)$.

Proof: See Appendix E. \square

Proposition 2 shows that the rate of convergence depends on the eigenvalues of $\hat{\mathbf{V}}^T \hat{\mathbf{V}}$ and $\hat{\mathbf{U}}^T \hat{\mathbf{U}}$, where $\hat{\mathbf{V}}$ and $\hat{\mathbf{U}}$ carry the location signatures of the source. Specifically, if the sources are aligned with either the x axis or the y axis, then either $\hat{\mathbf{U}}$ or $\hat{\mathbf{V}}$ tends to have identical columns, which leads to rank deficiency of matrices $\hat{\mathbf{U}}^T \hat{\mathbf{U}}$ or $\hat{\mathbf{V}}^T \hat{\mathbf{V}}$, corresponding to small eigenvalues λ_K and hence slow convergence.

Propositions 2 provides useful intuition for algorithm design; they show that gradient type algorithms work better when sources are well-separated in both axes.

D. Rotation for Convergence Improvement

As it is preferred to analyze the case where the sources are well-separated in both axes of the coordinate system, we may need to establish a coordinate system with the optimal rotation for the desired source topology. However, the challenge is that we have *no* prior knowledge of the source locations.

Recall that $\mathbf{H}(\theta)$ denotes the observation matrix constructed in coordinate system \mathcal{C}_θ with θ degrees of rotation with respect to the reference coordinate system \mathcal{C} . Similar to $\mathcal{P}3$, the desired rotation θ can be obtained as

$$\mathcal{P}4: \quad \underset{\theta \in [0, \frac{\pi}{2}]}{\text{minimize}} \quad \rho(\theta) \triangleq \frac{\sigma_1^2(\mathbf{H}(\theta))}{\sum_{k=1}^N \sigma_k^2(\mathbf{H}(\theta))} \quad (29)$$

where $\sigma_k(\mathbf{H})$ is defined as the k th largest singular value of $\hat{\mathbf{X}}(\mathbf{H})$, the solution to the matrix completion problem $\mathcal{P}2$ based on \mathbf{H} .

While problem $\mathcal{P}3$ is to align the sources with one of the axes, problem $\mathcal{P}4$ tries to avoid alignments with any axes.

Fig. 2 demonstrates the performance of the UMF with optimal coordinate system rotation under noise-free sampling $\sigma_n^2 = 0$, where $L = 1$ and the energy field is given by $h(d) = \sqrt{2\gamma/\pi} \exp(-\gamma d^2)$ with $\lambda = 20$. The observation matrices constructed with dimension N satisfy $N^2/2 \approx M$. There are two key observations: (i) the coordination system rotation does improve the convergence as demonstrated by the comparison between scheme ‘‘Rotated UMF’’, which solves $\mathcal{P}1$ in the optimal coordinate system \mathcal{C}_{θ^*} with θ^* solved from $\mathcal{P}4$, and scheme ‘‘Simple UMF’’, which solves $\mathcal{P}1$ in a fixed coordinate system \mathcal{C} . (ii) UMF performs better in the recovery of sparse unimodal structures as compared to conventional sparse matrix completion methods, scheme ‘‘Complete UMF’’, which first solves the matrix completion

⁴In fact, optimizing the value at the s th turning point may involve complexity scaling with N .

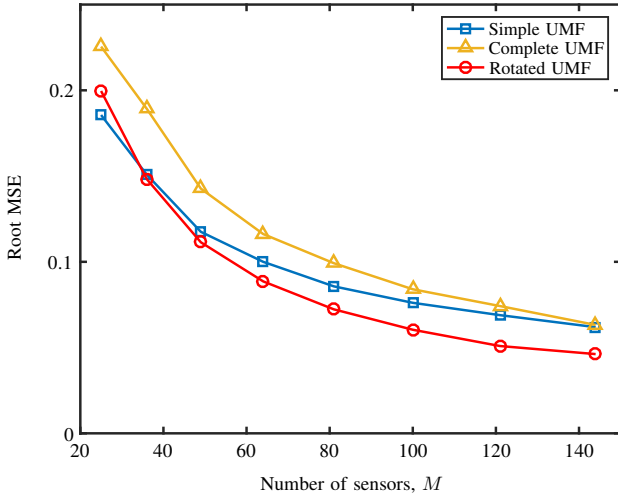


Figure 2. Localization performance under noise-free sampling in a two source Gaussian energy field.

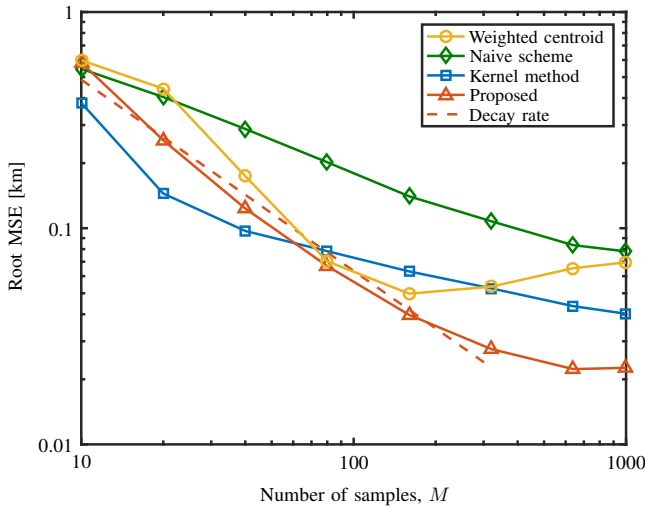


Figure 3. MSE of the source location versus the number of sensors, M , in the single source case.

problem $\mathcal{P}2$ in the optimal coordinate system \mathcal{C}_{θ^*} , and then solves $\mathcal{P}1$ for signature vector extraction. As the UMF is aware of the unimodal structure, the proposed “Rotated UMF” outperforms the “Complete UMF” scheme.⁵

VI. NUMERICAL RESULTS

We consider the source and sensor deployment model in Section II with $L = 5$ km in an underwater environment. The sources simultaneously transmit signals at $f = 5$ kHz. The propagation of the signal from each source is modeled using $N_p = 15$ discrete paths, where the path inter-arrival times $\tau_{p+1} - \tau_p$ are exponentially distributed with mean 100 ms, and the path amplitudes are Rayleigh distributed with power scaled as $e^{-\varphi(\tau_p - \tau_1)}$ with respect to the first path, $\varphi = 2 \text{ sec}^{-1}$ [21], [22]. The path energy attenuation is

⁵However, we also note that in the case of low SNR, i.e., $\sigma_n^2 \gg 1$, $\mathcal{P}2$ can serve as an efficient de-noising step to help faster convergence of UMF.

modeled as $(1 + d^{1.5}A(f)^d)^{-1}$, where Thorp’s formula [23] is used to arrive at $10 \log_{10} A(f) = 0.11f^2/(1 + f^2) + 44f^2/(4100 + f^2) + 2.75 \times 10^{-4}f^2 + 0.003$ dB/km. The ambient noise $n^{(m)}$ is modeled as a zero mean, Gaussian random variable with normalized variance $\sigma_n^2/P = -34$ dB, where $P = 1$ is the total transmission power. The sensor has a receive window of 4 seconds from the detection of the first path. The parameter N for constructing the observation matrix \mathbf{H} is chosen as the largest integer satisfying $N(\log N)^2 \leq M$.

The proposed algorithms for the single source case ((15) in Section III), two source ((21) – (23) in Section IV), and an arbitrary number of sources (Section V) are compared with two baseline schemes. Baseline 1, *Naive scheme for single source*: the location of the sensor that observes the highest energy is identified as the source location. Baseline 2, *Weighted centroid localization* [10]: the location estimate is updated by

$$\hat{\mathbf{s}}(n+1) = \frac{\sum_{m \in \mathcal{R}(\hat{\mathbf{s}}(n))} \varrho^{(m)} \mathbf{z}^{(m)}}{\sum_{m \in \mathcal{R}(\hat{\mathbf{s}}(n))} \varrho^{(m)}}$$

until convergence, where $\varrho^{(m)} = h^{(m)}$ are the weights and $\mathcal{R}(x)$ specifies a set of measurements that are taken within a radius r from location x , in which, the radius r is at least $L/8$ or as large as to include $M/4$ measurements. Baseline 3, *Kernel regression*: The algorithm chooses parameters $\{\alpha_k, \hat{\mathbf{z}}_k\}$ and λ to minimize $\sum_m |h^{(m)} - \sum_{k=1}^K \alpha_k B(\mathbf{z}^{(m)}, \hat{\mathbf{z}}_k; \lambda)|^2$ based on the measurement $\{h^{(m)}, \mathbf{z}^{(m)}\}$, where two classes of kernel functions are considered, Gaussian kernel $B_G(\mathbf{z}, \hat{\mathbf{z}}_k; \lambda) = \exp(-\lambda \|\mathbf{z} - \hat{\mathbf{z}}_k\|^2)$ and Laplacian kernel $B_L(\mathbf{z}, \hat{\mathbf{z}}_k; \lambda) = \exp(-\lambda \|\mathbf{z} - \hat{\mathbf{z}}_k\|_1)$, in which, $\|\cdot\|_1$ denotes the L_1 norm. Cross-validation is used to choose the best kernel function, and the data set is partitioned to 70% for parameter training and 30% for MSE performance validation. The parameters $\hat{\mathbf{z}}_k$ give the location estimates. Note that Baselines 1 and 2 cannot differentiate multiple sources when they appear as one. Therefore, these two baselines are evaluated in the single source case only.

Fig. 3 shows the rooted mean squared error (RMSE) of the source location versus the number of sensors, M , in the single source case. The proposed scheme outperforms the naive scheme and the weighted centroid scheme.⁶ It also outperforms the kernel method from moderate to large number of sensors. In the case of more than 500 sensors, the performance is limited by the ambient noise. The dashed line fits the performance of the proposed scheme in the $M = 10$ to 500 region using $\log_{10} \text{RMSE} = a \log_{10} M + b$. It gets $a = -0.88$ and hence the MSE decreases as $\mathcal{O}(1/M^{1.76})$. Note that Theorem 2 and 3 show that the MSE of the proposed scheme should decrease faster than $\mathcal{O}(1/M^{1.5})$ (full sampling case), which is confirmed by our numerical results.

Fig. 4 shows the RMSE of the source locations versus the number of sensors, M , in two source and three source cases. In both cases, the proposed methods significantly outperform the kernel methods. Note that the proposed schemes only require

⁶It is observed from our numerical experiments that the weights ϱ and the window \mathcal{R} in the weighted centroid scheme should depend on M and $h(d)$. However, choosing the best weights and window are highly non-trivial.

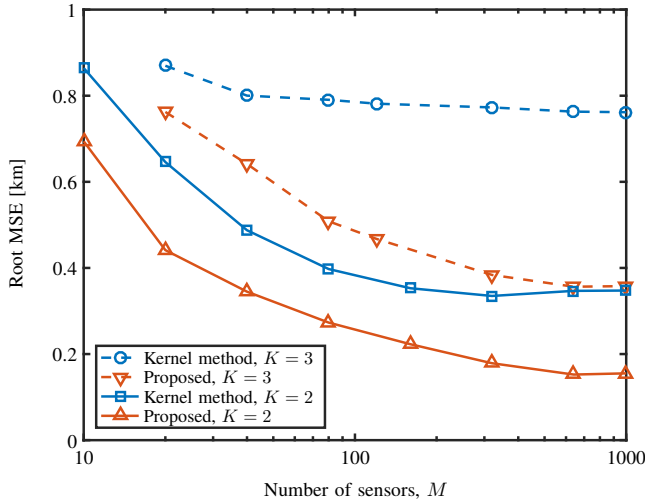


Figure 4. MSE of the source location versus the number of sensors, M , in two source and three source cases.

the generic property that the source energy field $h(d)$ is non-negative and strictly decreasing in the distance d to the source. Although the kernel functions also capture such property, the kernel methods suffer from parameter estimation error when fitting the data to inaccurate parametric models.

Fig. 5 demonstrates the robustness of the proposed method in localizing several peaks on real data. The dataset contains altitude data (colored pixels) measured on the road networks in North Jutland, Denmark [24], where red pixels represent high altitude locations. Such an altitude dataset is selected to emulate noise-corrupted measurements of an energy field generated by $K = 3$ hidden sources. We downsample the dataset over 40×40 equally spaced grid points and form a sparse elevation matrix. We find the peaks (black triangles) by solving $\mathcal{P}1$ to extract the signature vectors followed by peak localization using (15). The result matches with a visual determination of possible locations of the hidden sources.⁷

VII. CONCLUSIONS

This paper developed nonparametric algorithms for localizing multiple sources based on a moderate number of energy measurements from different locations. A matrix observation model was proposed and proven to have unimodal and symmetric properties for every energy field under mild conditions. A nonparametric source localization algorithm exploiting the unimodal and symmetric property was developed and shown to decrease the localization MSE faster than $\mathcal{O}(1/M^{1.5})$ using M sensors in the single source case. In the two source case, the source locations can be found by choosing the optimal rotation of the coordinate system such that the normalized dominant singular value of the sample matrix is maximized. In the case of arbitrary number of sources, we localize the sources by solving a UMF problem in an optimally rotated

⁷In this experiment, we failed to successfully implement the kernel regression method to localize the peaks. There are too many local optima of the nonlinear regression problem, and furthermore, the local optima are not necessarily consistent with the peak locations.

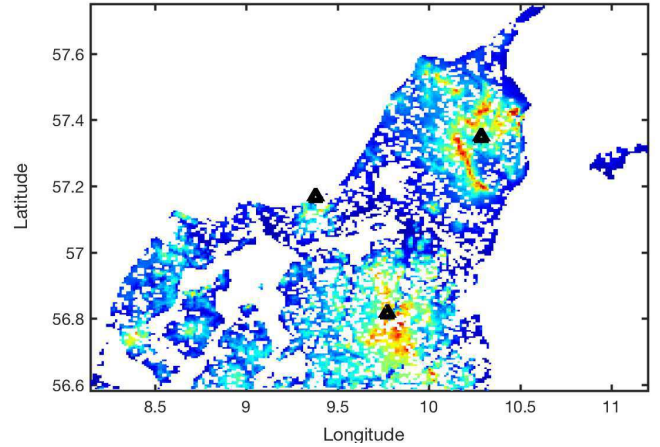


Figure 5. Localizing the three peaks from the elevation data of North Jutland, Denmark. The result matches with the visual expectation.

coordinate system. Our numerical experiments demonstrate that the proposed scheme achieves similar performance as the baselines using no more than $1/5$ measurement samples.

APPENDIX A PROOF OF THEOREM 1

As the signature vectors \mathbf{u}_k and \mathbf{v}_k correspond to the dominant singular vectors $\mathbf{u}_{k,1}$ and $\mathbf{v}_{k,1}$ of $\mathbf{H}^{(k)}$, we can focus on only one source and drop the source index k here for brevity. Specifically, from (4), we write $\mathbf{H} = \alpha \mathbf{u} \mathbf{v}^T + \sum_{i=2}^N \lambda_i \mathbf{u}_i \mathbf{v}_i^T$ (for the k th source, where $k = 1$), in which \mathbf{u} and \mathbf{u}_i are the left singular vectors of \mathbf{H} , \mathbf{v} and \mathbf{v}_i are the right singular vectors, and α is the largest singular value, $\alpha > \lambda_i$, $i = 2, 3, \dots, N$.

Let $\mathbf{R} = \mathbf{H}^T \mathbf{H}$. Then, the (i, j) th entry of \mathbf{R} is given by $R_{ij} = \mathbf{h}_i^T \mathbf{h}_j$, where \mathbf{h}_i is the i th column of \mathbf{H} . In the following lemma, we show that the columns of \mathbf{R} are unimodal.

Lemma 2. *Suppose that the source locates at the (m, n) th grid centered at $\mathbf{c}_{m,n}$. Then, for each column of \mathbf{R} , the entries R_{ij} are increasing, $R_{ij} < R_{i+1,j}$, if $i < n$, and they are decreasing, $R_{ij} > R_{i+1,j}$, if $i \geq n$.*

Proof: Since the source location \mathbf{s} is inside the (m, n) th grid centered at $\mathbf{c}_{m,n}$, we have $d(\mathbf{c}_{p,i}, \mathbf{s}) > d(\mathbf{c}_{p,i+1}, \mathbf{s}) \geq d(\mathbf{c}_{p,n}, \mathbf{s})$, for $i < n$ and all $p = 1, 2, \dots, N$. Similarly, $d(\mathbf{c}_{p,i}, \mathbf{s}) < d(\mathbf{c}_{p,i+1}, \mathbf{s})$, for $i \geq n$ and all p . Recall that $H_{ij} = h(d(\mathbf{c}_{i,j}, \mathbf{s}))$ and $h(d)$ is a non-negative decreasing function. We thus have

$$\begin{aligned} R_{ij} &= \mathbf{h}_i^T \mathbf{h}_j = \sum_{p=1}^N H_{pi} H_{pj} \\ &< \sum_{p=1}^N H_{p,i+1} H_{pj} = \mathbf{h}_{i+1}^T \mathbf{h}_j = R_{i+1,j} \end{aligned}$$

for $i < n$. Similarly, we can show that $R_{ij} = \mathbf{h}_i^T \mathbf{h}_j > \mathbf{h}_{i+1}^T \mathbf{h}_j = R_{i+1,j}$, for $i \geq n$. \square

Under the condition of Lemma 2, if we raise \mathbf{R} to the power of q , the columns of \mathbf{R}^q are unimodal, with their peaks at

the n th entry. Specifically, define $\mathbf{R}^{(q)} \triangleq \mathbf{R}^q / \text{tr}\{\mathbf{R}^q\}$. We show, in the following lemma, that the columns of $\mathbf{R}^{(q)}$ are unimodal.

Lemma 3. *Let $R_{ij}^{(q)}$ be the (i, j) th entry of $\mathbf{R}^{(q)}$. Then, $R_{ij}^{(q)} < R_{i+1,j}^{(q)}$, if $i < n$, and $R_{ij}^{(q)} > R_{i+1,j}^{(q)}$, if $i \geq n$.*

Proof: First, it can be easily verified that the result holds for $q = 1$ according to Lemma 2. Then, suppose that the result holds for some $q \geq 1$. Note that $\mathbf{R}^{(q+1)} = \text{tr}\{\mathbf{R}^{(q)}\} \mathbf{R}^{(q)} / \text{tr}\{\mathbf{R}^{(q+1)}\}$ and that $\mathbf{R}^{(q)}$ is symmetric. We have

$$\begin{aligned} R_{ij}^{(q+1)} &= \frac{\text{tr}\{\mathbf{R}^q\}}{\text{tr}\{\mathbf{R}^{q+1}\}} \sum_{p=1}^N R_{pi}^{(q)} R_{pj} \\ &< \frac{\text{tr}\{\mathbf{R}^q\}}{\text{tr}\{\mathbf{R}^{q+1}\}} \sum_{p=i+1}^N R_{p,i+1} R_{pj} = R_{i+1,j}^{(q+1)} \end{aligned}$$

for $i < n$. Similarly, we can show that $R_{ij}^{(q+1)} > R_{i+1,j}^{(q+1)}$, for $i \geq n$. Therefore, by deduction, the result holds for all $q \geq 1$. \square

Let $\mathbf{R}^\infty \triangleq \lim_{q \rightarrow \infty} \mathbf{R}^q / \text{tr}\{\mathbf{R}^q\}$. It can be shown that the limit exists and equals $\mathbf{R}^\infty = \mathbf{v}\mathbf{v}^\top$. To see this, we can easily compute $\mathbf{R}^q = \alpha^{2q} \mathbf{v}\mathbf{v}^\top + \sum_{i=2}^N \lambda_i^{2q} \mathbf{v}_i \mathbf{v}_i^\top$ and the normalization term $\text{tr}\{\mathbf{R}^q\} = (\alpha^{2q} + \sum_{i=2}^N \lambda_i^{2q})$, and note that $(\lambda_i/\alpha)^{2q} \rightarrow 0$ as $q \rightarrow \infty$, for $i = 2, 3, \dots, N$, leading to \mathbf{R}^∞ being rank-1.

On the other hand, from Lemma 3, each column of \mathbf{R}^∞ is unimodal. Note that the i th column of \mathbf{R}^∞ can be written as $v_i \mathbf{v}$, where v_i is the i th entry of \mathbf{v} . We therefore confirm that \mathbf{v} is unimodal, with its n th entry being the peak.

Similarly, by constructing $\mathbf{Q} = \mathbf{H}\mathbf{H}^\top$, we can also show that \mathbf{u} is unimodal with its m th entry being the peak. \square

APPENDIX B

PROOF OF PROPOSITION 1

Consider a slight shift of the grids $\hat{\mathbf{c}}_{i,j} = \mathbf{c}_{i,j} + [\delta_1, \delta_2]$, and denote $\hat{\mathbf{c}}_X = \mathbf{c}_X + \delta_1$ and $\hat{\mathbf{c}}_Y = \mathbf{c}_Y + \delta_2$. As a result, the source locates exactly at the center of the (m, n) th grid, i.e., $\mathbf{s}_k = \hat{\mathbf{c}}_{m,n}$.

Let $\hat{\mathbf{H}}^{(k)}$ be the signature matrix measured at the shifted grids $\{\hat{\mathbf{c}}_{i,j}\}$. Then, we have

$$\begin{aligned} |H_{ij}^{(k)} - \hat{H}_{ij}^{(k)}| &= \frac{L}{N} \left| h(d_{ij}) - \left(h(d_{ij}) + \int_0^1 h'(d_{ij} + t\hat{\delta}_{ij}) dt \right) \right| \\ &\leq \frac{K_h L}{N} |\hat{\delta}_{ij}| \\ &\leq \frac{K_h L^2}{\sqrt{2} N^2} \end{aligned}$$

where $d_{ij} = \|\mathbf{c}_{i,j} - \mathbf{s}_k\|$, $\hat{\delta}_{ij} = \|\hat{\mathbf{c}}_{i,j} - \mathbf{s}_k\| - d_{ij}$, and $h'(d) = \lim_{t \downarrow 0} \frac{1}{t} [h(d+t) - h(d)]$ denotes the right derivative of $h(d)$.

Consider the largest sub-block $[\hat{\mathbf{H}}^{(k)}]_J$ of $\hat{\mathbf{H}}^{(k)}$ that includes rows $m-J$ to $m+J$, and columns $n-J$ to $n+J$ for the largest possible integer J . The sub-matrix $[\hat{\mathbf{H}}^{(k)}]_J$ then has dimension $(2J+1) \times (2J+1)$. In addition, the sub-matrix is symmetric about the $(J+1, J+1)$ th entry, where the j th row and $(2J+2-j)$ th row are identical, and the j th column and the $(2J+2-j)$ th column are identical.

This is because the grids $\hat{\mathbf{c}}_{m-i,n-j}$, $\hat{\mathbf{c}}_{m+i,n-j}$, $\hat{\mathbf{c}}_{m-i,n+j}$, and $\hat{\mathbf{c}}_{m+i,n+j}$ have equal distance to the source $\mathbf{s}_k = \hat{\mathbf{c}}_{m,n}$, and thus the corresponding entries $\hat{H}_{pq}^{(k)}$ are identical.

As a result, the rank-1 sub-matrix $[\hat{\mathbf{H}}^{(k)}]_{\mathcal{J}_m \times \mathcal{J}_n}$ has symmetric singular vectors that satisfy $[\hat{\mathbf{u}}_k]_{\mathcal{J}_m} = [\hat{\mathbf{v}}_k]_{\mathcal{J}_n}$, and the singular vectors are symmetric about the $(J+1)$ th entry, where \mathcal{J}_m and \mathcal{J}_n are some index sets that contain $2J+1$ elements, respectively. Note that vectors $[\hat{\mathbf{u}}_k]_{\mathcal{J}_m}$ and $[\hat{\mathbf{v}}_k]_{\mathcal{J}_n}$ are sub-blocks of the singular vectors $\hat{\mathbf{u}}_k$ and $\hat{\mathbf{v}}_k$ of the rank-1 full matrix $\hat{\mathbf{H}}^{(k)}$, respectively. We thus know that $\hat{\mathbf{u}}_k$ and $\hat{\mathbf{v}}_k$ are symmetric vectors about the m th entry and n th entry, respectively. Moreover, $\hat{\mathbf{u}}_k$ and $\hat{\mathbf{v}}_k$ are unimodal by Theorem 1.

Therefore, w.l.o.g., assume $m < n \leq N/2$. We can theoretically construct a continuous function $w(x)$ that takes value $w(x) = \sqrt{N/L} \hat{v}_{k,j}$ for $x = \hat{\mathbf{c}}_{X,j} - s_{k,1}$ and $j = 1, 2, \dots, n-1$, $w(x) = \sqrt{N/L} \hat{u}_{k,i}$ for $x = \hat{\mathbf{c}}_{Y,i} - s_{k,2}$ and $i = m, m+1, \dots, N$, and by smooth interpolation elsewhere such that $w(x)$ is non-negative, unimodal, and symmetric about $x = 0$. \square

APPENDIX C

PROOF OF THEOREM 2

We first compute the peak localization error bound given signature vector perturbations.

Let $\hat{\mathbf{v}}_1$ be the dominant right singular vectors of \mathbf{H} , the observation matrix in the case of conservative construction, $N = \sqrt{M}$. In the case of aggressive construction, $N > \sqrt{M}$, let $\hat{\mathbf{v}}_1$ be the dominant right singular vector of $\hat{\mathbf{X}}$, the solution to $\mathcal{P}2$. Denote $\mathbf{e}_1 = \hat{\mathbf{v}}_1 - \mathbf{v}_1$.

Recall that the signature vector \mathbf{v}_1 can be approximately expressed as a discretization of $w(x - s_{1,1})$ from Proposition 1, and in addition, $e(x) = \hat{v}(x) - w(x - s_{1,1})$ is the error of the continuous non-parametric regression $\hat{v}(x)$ obtained from interpolating $\hat{\mathbf{v}}_1$. We denote $w_1(x) = w(x - s_{1,1})$ for the ease of elaboration. From (16), it follows that

$$\begin{aligned} R(t; \hat{\mathbf{v}}_1) &= \int_{-\infty}^{\infty} (w_1(x) + e(x)) (w_1(-x+t) + e(-x+t)) dx \\ &= \int_{-\infty}^{\infty} w_1(x) w_1(-x+t) dx + \int_{-\infty}^{\infty} w_1(x) e(-x+t) dx \\ &\quad + \int_{-\infty}^{\infty} e(x) w_1(-x+t) dx + \int_{-\infty}^{\infty} e(x) e(-x+t) dx \\ &\approx \tau(t - 2s_{1,1}) + \int_{-\infty}^{\infty} w_1(x) e(-x+t) dx \\ &\quad + \int_{+\infty}^{-\infty} e(-y+t) w_1(y) (-dy) \\ &= \tau(t - 2s_{1,1}) + 2 \int_{-\infty}^{\infty} w_1(x) e(-x+t) dx \end{aligned} \tag{30}$$

$$= \tau(t - 2s_{1,1}) + 2 \int_{-\infty}^{\infty} w_1(x) e(-x+t) dx \tag{31}$$

where the approximation (30) drops the second order term $\int_{-\infty}^{\infty} e(x) e(-x+t) dx$ and uses the fact that $\int_{-\infty}^{\infty} w_1(x) w_1(-x+t) dx = \tau(t - 2s_{1,1})$ from the integral (12).

As $t = 2\hat{s}_{1,1}$ maximizes $R(t; \hat{\mathbf{v}}_1)$ in (31), we have

$$\begin{aligned} \tau(2\hat{s}_{1,1} - 2s_{1,1}) + 2 \int_{-\infty}^{\infty} w_1(x) e(-x + 2\hat{s}_{1,1}) dx \\ \geq \tau(2s_{1,1} - 2s_{1,1}) + 2 \int_{-\infty}^{\infty} w_1(x) e(-x + 2s_{1,1}) dx \\ = \tau(0) + 2 \int_{-\infty}^{\infty} w_1(x) e(-x + 2s_{1,1}) dx \end{aligned}$$

where $\tau(0) = \int_{-\infty}^{\infty} w_1(x)^2 dx \approx \sum_j v_{1,j}^2 = 1$. As a result,

$$\begin{aligned} \tau(0) - \tau(2\hat{s}_{1,1} - 2s_{1,1}) \\ \leq 2 \int_{-\infty}^{\infty} w_1(x) \left[e(-x + 2\hat{s}_{1,1}) - e(-x + 2s_{1,1}) \right] dx \\ \leq 2C_e \left| \int_{-\infty}^{\infty} w_1(x) e(x) dx \right| \\ \approx 2C_e \sum_j v_{1,j} e_{1,j} \\ = 2C_e |\mathbf{v}_1^T \mathbf{e}_1|. \end{aligned}$$

In addition, using the Taylor's expansion of $\tau(t)$ at $t = 0$, we have

$$\begin{aligned} \tau(2\hat{s}_{1,1} - 2s_{1,1}) \\ \approx \tau(0) + \tau(0)' \times 2(\hat{s}_{1,1} - s_{1,1}) + \frac{1}{2} \tau(0)'' \times 4(\hat{s}_{1,1} - s_{1,1})^2 \\ \geq \tau(0) - 2C_e |\mathbf{v}_1^T \mathbf{e}_1| \end{aligned}$$

where, it can be verified that the first order derivative $\tau(0)' = 0$ and the second order derivative $\tau''(0) < 0$ by the definition of $\tau(t)$ in (11). As a result,

$$(\hat{s}_{1,1} - s_{1,1})^2 \leq \frac{C_e}{-\tau''(0)} |\mathbf{v}_1^T \mathbf{e}_1| \quad (32)$$

for asymptotically large N (since all the approximations become accurate for large N).

Similar result can be derived for $(\hat{s}_{1,2} - s_{1,2})^2$ by analyzing the perturbation of \mathbf{u}_1 , and the result is statistically identical to (32). Therefore, the squared error bound is given by (as $\tau''(0) < 0$)

$$\|\hat{\mathbf{s}}_1 - \mathbf{s}_1\|_2^2 \leq \frac{2C_e}{|\tau''(0)|} |\mathbf{v}_1^T \mathbf{e}_1|.$$

We now derive the signature perturbation $|\mathbf{v}_1^T \mathbf{e}_1|$ by discussing two cases.

A. The Case of Conservative Construction $N = \sqrt{M}$

Consider that the sensing location $\mathbf{z}^{(m)}$ is inside the grid centered at $\mathbf{c}_{i,j}$. Then, according to the matrix observation model (1), (2), and (7), we have

$$\begin{aligned} (H_{ij} - H_{ij})^2 &= \frac{L^2}{N^2} \left(h^{(m)} - \alpha_1 h(d_{ij}) \right)^2 \\ &= \alpha_1^2 \frac{L^2}{N^2} \left(\int_0^1 h'(d_{ij} + t\delta^{(m)}) dt + \frac{\mathbf{n}^{(m)}}{\alpha_1} \right)^2 \\ &= \frac{\alpha_1^2 L^2}{N^2} \left(\Xi^2 + 2\Xi \frac{\mathbf{n}^{(m)}}{\alpha_1} + \left(\frac{\mathbf{n}^{(m)}}{\alpha_1} \right)^2 \right) \quad (33) \end{aligned}$$

where $d_{ij} = \|\mathbf{c}_{i,j} - \mathbf{s}_1\|_2$, $\delta^{(m)} = \|\mathbf{z}^{(m)} - \mathbf{s}_1\|_2 - d_{ij}$, $h'(d) = \lim_{t \downarrow 0} \frac{1}{t} [h(t+d) - h(d)]$ is the right derivative of $h(d)$, and $\Xi \triangleq \int_0^1 h'(d_{ij} + t\delta^{(m)}) dt$.

Note that by the Lipschitz continuity of $h(d)$, we have $|\Xi| \leq K_h \delta^{(m)} \leq K_h L / (\sqrt{2}N)$. Therefore,

$$\mathbb{E} \left\{ (H_{ij} - H_{ij})^2 \right\} \leq \frac{\alpha_1^2 K_h^2 L^4}{2N^4} + \frac{\alpha_1^2 L^2 \sigma_n^2}{N^2 \alpha_1^2} \triangleq \omega^2 \quad (34)$$

Using (34), we now derive an upper bound of $|\mathbf{v}_1^T \mathbf{e}_1|$.

Note that $\mathbf{v}_1^T \mathbf{e}_1 < 0$ because $1 = \|\hat{\mathbf{v}}_1\|_2^2 = \|\mathbf{v}_1 + \mathbf{e}_1\|_2^2 = 1 + 2\mathbf{v}_1^T \mathbf{e}_1 + \|\mathbf{e}_1\|_2^2$, and hence, $2\mathbf{v}_1^T \mathbf{e}_1 = -\|\mathbf{e}_1\|_2^2 < 0$. Then, the singular vector perturbation can be obtained as

$$\begin{aligned} \sin \angle(\mathbf{v}_1, \hat{\mathbf{v}}_1) &= \sqrt{1 - |\mathbf{v}_1^T (\mathbf{v}_1 + \mathbf{e}_1)|^2} \\ &= \sqrt{-2\mathbf{v}_1^T \mathbf{e}_1 + (\mathbf{v}_1^T \mathbf{e}_1)^2} \\ &\geq \sqrt{2|\mathbf{v}_1^T \mathbf{e}_1|} \quad (35) \end{aligned}$$

where $|\cdot|$ denotes the absolute value operator.

Let $\mathbf{E} = \mathbf{H} - \mathbf{H}$. Using the singular vector perturbation results in [25], we know that

$$\sin \angle(\mathbf{v}_1, \hat{\mathbf{v}}_1) \leq \frac{2\sigma(\mathbf{E})}{\sigma_1 - \sigma_2} \quad (36)$$

where $\sigma(\mathbf{E})$ is the spectral norm of \mathbf{E} , and σ_1 and σ_2 are the first and second dominant singular values of \mathbf{H} . Note that we have $\sigma_1 - \sigma_2 = \kappa \alpha_1$.

We now compute $\sigma(\mathbf{E})$. From the uniform random sampling strategy for \mathbf{H} , the elements of \mathbf{E} are independent random variables with zero mean and variance strictly smaller than ω^2 in (34). Let $\bar{\mathbf{E}}$ be an $N \times N$ matrix whose elements are i.i.d. random variables with zero mean, variance ω^2 and bounded fourth order moment. Then we know that the spectral norm $\sigma(\mathbf{E}) < \sigma(\bar{\mathbf{E}})$ almost surely for asymptotically large N . On the other hand, using random matrix theory, it has been shown in [26, Theorem 2.1] that $\frac{1}{\omega\sqrt{N}} \sigma(\bar{\mathbf{E}}) \rightarrow 2$ almost surely, as $N \rightarrow \infty$. As a result, we have

$$\sigma(\mathbf{E})^2 < \sigma(\bar{\mathbf{E}})^2 \approx 4\omega^2 N \quad (37)$$

almost surely.

Combining the results in (35) – (37), we have

$$|\mathbf{v}_1^T \mathbf{e}_1| \leq \frac{1}{2} \left(\frac{2\sigma(\mathbf{E})}{\kappa \alpha_1} \right)^2 \approx \frac{4K_h^2 L^4}{\kappa^2 N^3} + \frac{8L^2 \sigma_n^2}{\kappa^2 N \alpha_1^2} \quad (38)$$

for asymptotically large N , almost surely.

B. The Case of Aggressive Construction $N > \sqrt{M}$

We first characterize the completed matrix $\hat{\mathbf{X}}$ as the solution to $\mathcal{P}2$.

Lemma 4 (Matrix completion with noise [19]). *Suppose that the parameter ϵ in $\mathcal{P}2$ is chosen to satisfy $\epsilon \geq \|\mathcal{P}_\Omega(\mathbf{H} - \mathbf{H})\|_F$. In addition, assume the N is the largest integer chosen such that $M \geq \beta C N (\log N)^2$ for some constant C . Then, with high probability,*

$$\eta \triangleq \|\hat{\mathbf{X}} - \mathbf{H}\|_F \leq 4 \sqrt{\frac{(2+p)N}{p}} \epsilon + 2\epsilon \quad (39)$$

where $p = M/N^2$.

Using (33), we have

$$(H_{ij} - H_{ij})^2 \leq \frac{\alpha_1^2 L^2}{N^2} \left(\frac{K_h^2 L^2}{2N^2} + \frac{\sqrt{2}K_h L \bar{\sigma}_n}{N \alpha_1} + \frac{\bar{\sigma}_n^2}{\alpha_1^2} \right) \triangleq \bar{\epsilon}^2.$$

Using the fact that

$$\|\mathcal{P}_\Omega(\mathbf{H} - \mathbf{H})\|_{\mathbb{F}}^2 = \sum_{(i,j) \in \Omega} |H_{ij} - H_{ij}|^2 \leq M \bar{\epsilon}^2$$

the choice of parameter $\epsilon = \sqrt{M} \bar{\epsilon}$, and $M \approx \beta CN(\log N)^2$ for asymptotically large N , the bound (39) can be simplified as

$$\begin{aligned} \eta &\leq 4 \sqrt{\frac{(2 + \beta CN(\log N)^2/N^2)N}{CN(\log N)^2/N^2}} \sqrt{M} \bar{\epsilon} + 2\sqrt{M} \bar{\epsilon} \\ &\approx \sqrt{\frac{32}{\beta C \log N}} \frac{N}{\sqrt{M} \bar{\epsilon}} \\ &\triangleq \bar{\eta}. \end{aligned} \quad (40)$$

Let $\hat{\mathbf{E}}$ be an $N \times N$ matrix, where the elements are i.i.d. random variables with zero mean and variance $\tilde{\omega}^2 = \bar{\eta}^2/N^2$, and bounded fourth order moment. As a result, we have $\mathbb{E}\{\|\hat{\mathbf{E}}\|_{\mathbb{F}}^2\} \geq \|\hat{\mathbf{X}} - \mathbf{H}\|_{\mathbb{F}}^2$ with probability 1. Therefore, using the results in [26, Theorem 2.1], the spectral norm of $\hat{\mathbf{E}}$ converges to $\frac{1}{\sqrt{N}} \sigma(\hat{\mathbf{E}}) \rightarrow 2$ almost surely as $N \rightarrow \infty$. As a result,

$$\sigma(\hat{\mathbf{X}} - \mathbf{H})^2 < \sigma(\hat{\mathbf{E}})^2 \approx 4\tilde{\omega}^2 N$$

almost surely.

Using the singular vector perturbation results in [25] and following similar calculations in (35) – (38), we have

$$|\mathbf{v}_1^T \mathbf{e}_1| \leq \frac{1}{2} \left(\frac{2\sigma(\hat{\mathbf{E}})}{\kappa \alpha_1} \right)^2 \approx \frac{256L^2}{\kappa^2} \left(\frac{K_h^2 L^2}{2N^2} + \frac{\sqrt{2}K_h L \bar{\sigma}_n}{N \alpha_1} + \frac{\bar{\sigma}_n^2}{\alpha_1^2} \right).$$

APPENDIX D PROOF OF THEOREM 4

W.l.o.g., assume that the two sources locate at $\mathbf{s}_1 = (0, 0)$ and $\mathbf{s}_2 = (D \cos \theta, D \sin \theta)$. Define $w_c(x, \theta) = w(x - D \cos \theta)$ and $w_s(x, \theta) = w(x - D \sin \theta)$, where $w(x)$ is the unimodal and symmetric function defined in Proposition 1. In addition, using (3), we have $\int_{-\infty}^{\infty} w(x)^2 dx \approx 1$.

Using Proposition 1, we have the following approximation

$$\begin{aligned} \|\mathbf{u}_1 + \mathbf{u}_2\|_2^2 &\approx \int_{-\infty}^{\infty} (w(x) + w_c(x, \theta))^2 dx \\ &\triangleq \langle (w + w_c)^2 \rangle \end{aligned}$$

where we have defined an integration operator $\langle \cdot \rangle$ as

$$\langle f \rangle \triangleq \int_{-\infty}^{\infty} f(x, \theta) dx$$

for a function $f(x, \theta)$. Note that the operator $\langle \cdot \rangle$ is linear and satisfies the additive property, i.e., $\langle af \rangle = a \langle f \rangle$ and $\langle f + g \rangle = \langle f \rangle + \langle g \rangle$, for a constant a and a function $g(x, \theta)$.

Similarly, $\|\mathbf{v}_1 + \mathbf{v}_2\|_2^2 \approx \langle (w + w_s)^2 \rangle$, $\|\mathbf{u}_1 - \mathbf{u}_2\|_2^2 \approx \langle (w - w_c)^2 \rangle$, and $\|\mathbf{v}_1 - \mathbf{v}_2\|_2^2 \approx \langle (w - w_s)^2 \rangle$.

In the case of $\alpha_1 = \alpha_2$, it can be shown that the SVD of \mathbf{H} is given by

$$\mathbf{H} = \sigma_1 \mathbf{p}_1 \mathbf{q}_1^T + \sigma_2 \mathbf{p}_2 \mathbf{q}_2^T \quad (41)$$

where $\sigma_1(\theta) = \frac{1}{2} \alpha_1 \|\mathbf{u}_1 + \mathbf{u}_2\|_2 \|\mathbf{v}_1 + \mathbf{v}_2\|_2$ and $\sigma_2(\theta) = \frac{1}{2} \alpha_1 \|\mathbf{u}_1 - \mathbf{u}_2\|_2 \|\mathbf{v}_1 - \mathbf{v}_2\|_2$ are the singular values, and

$$\begin{aligned} \mathbf{p}_1 &= \frac{\mathbf{u}_1 + \mathbf{u}_2}{\|\mathbf{u}_1 + \mathbf{u}_2\|_2}, & \mathbf{q}_1 &= \frac{\mathbf{v}_1 + \mathbf{v}_2}{\|\mathbf{v}_1 + \mathbf{v}_2\|_2} \\ \mathbf{p}_2 &= \frac{\mathbf{u}_1 - \mathbf{u}_2}{\|\mathbf{u}_1 - \mathbf{u}_2\|_2}, & \mathbf{q}_2 &= \frac{\mathbf{v}_1 - \mathbf{v}_2}{\|\mathbf{v}_1 - \mathbf{v}_2\|_2} \end{aligned}$$

are the corresponding singular vectors. Here, all the components are functions of θ .

As a result,

$$\begin{aligned} \mu(\theta) &\triangleq \frac{\sigma_2(\theta)^2}{\sigma_1(\theta)^2} \\ &\approx \frac{\langle (w - w_c)^2 \rangle \langle (w - w_s)^2 \rangle}{\langle (w + w_c)^2 \rangle \langle (w + w_s)^2 \rangle} \\ &= \frac{(1 - \langle w \cdot w_c \rangle)(1 - \langle w \cdot w_s \rangle)}{(1 + \langle w \cdot w_c \rangle)(1 + \langle w \cdot w_s \rangle)} \end{aligned} \quad (42)$$

where we have used the fact that $\langle (w - w_c)^2 \rangle = \langle w^2 \rangle + \langle w_c^2 \rangle - 2\langle w \cdot w_c \rangle = 2(1 - \langle w \cdot w_c \rangle)$.

In addition, from properties of calculus, if $f(x, \theta)$ and $\frac{\partial}{\partial \theta} f(x, \theta)$ are continuous in θ , then

$$\begin{aligned} \frac{d}{d\theta} \langle f \rangle &= \frac{d}{d\theta} \int_{-\infty}^{\infty} f(x, \theta) dx \\ &= \int_{-\infty}^{\infty} \frac{\partial}{\partial \theta} f(x, \theta) dx = \left\langle \frac{\partial}{\partial \theta} f \right\rangle. \end{aligned}$$

Therefore, defining

$$\begin{aligned} w'_c(x, \theta) &\triangleq \frac{d}{dx} w(x) \Big|_{x=x-D \cos \theta} \\ w'_s(x, \theta) &\triangleq \frac{d}{dx} w(x) \Big|_{x=x-D \sin \theta} \end{aligned}$$

we have

$$\begin{aligned} \frac{d}{d\theta} \langle w \cdot w_c \rangle &= \langle w \cdot \frac{\partial}{\partial \theta} w_c(x, \theta) \rangle = \langle w \cdot w'_c \rangle D \sin \theta \\ \frac{d}{d\theta} \langle w \cdot w_s \rangle &= \langle w \cdot \frac{\partial}{\partial \theta} w_s(x, \theta) \rangle = -\langle w \cdot w'_s \rangle D \cos \theta. \end{aligned}$$

With some algebra, the derivative of $\mu(\theta)$ can be obtained as

$$\begin{aligned} \frac{d}{d\theta} \mu(\theta) &= \eta \left[D \cos \theta \langle w \cdot w'_s \rangle (1 - \langle w \cdot w_c \rangle^2) \right. \\ &\quad \left. - D \sin \theta \langle w \cdot w'_c \rangle (1 - \langle w \cdot w_s \rangle^2) \right] \\ &= \eta \left[-t \cdot \tau'(s) (1 - \tau(t)^2) + s \cdot \tau'(t) (1 - \tau(s)^2) \right] \end{aligned}$$

where $\eta = 2(1 + \langle w \cdot w_c \rangle)^{-2} (1 + \langle w \cdot w_s \rangle)^{-2}$, $t = D \cos \theta$, and $s = D \sin \theta$.

Note that $0 < s < t$ for $0 < \theta < \frac{\pi}{4}$. Applying condition (20), we have

$$\begin{aligned} \frac{d}{d\theta} \mu(\theta) &> \eta \cdot t \cdot \tau'(s) \left[(1 - \tau(s)^2) - (1 - \tau(t)^2) \right] \\ &= \eta \cdot t \cdot \tau'(s) (\tau(t)^2 - \tau(s)^2) \\ &> 0 \end{aligned}$$

since $\tau'(s) < 0$ and $\tau(t) < \tau(s)$ for $0 < s < t$.

This confirms that $\mu(\theta)$ is a strictly increasing function, and hence $\rho(\theta)$ is a strictly decreasing function in $\theta \in (0, \frac{\pi}{4})$. The result is thus proved.

APPENDIX E PROOF OF PROPOSITION 2

For notation brevity, we drop the symbol t for the variables related to the continuous-time algorithm dynamic $\mathbf{X}(t)$ wherever the meaning is clear.

Denote the Hessian function of $f(\mathbf{X})$ along the direction $\boldsymbol{\xi} \in \mathbb{R}^{N \times N}$ as

$$h(\boldsymbol{\xi}, \mathbf{X}) = \lim_{\gamma \rightarrow 0} \frac{1}{\gamma} \left[g(\mathbf{X} + \gamma \boldsymbol{\xi}) - g(\mathbf{X}) \right].$$

Then, a Taylor's expansion of the gradient function $g(\mathbf{X})$ yields

$$g(\mathbf{X}) = g(\hat{\mathbf{X}}) + h(s\boldsymbol{\xi}, \hat{\mathbf{X}}) + o(s)$$

where $\boldsymbol{\xi} = \frac{1}{\gamma}(\mathbf{X} - \hat{\mathbf{X}})$ and $\gamma = \|\mathbf{X} - \hat{\mathbf{X}}\|_F$. Therefore, as $g(\hat{\mathbf{X}}) = \mathbf{0}$, it holds that $g(\mathbf{X}) \approx h(\mathbf{X}_e, \hat{\mathbf{X}})$ for small s .

In addition, it holds that

$$\begin{aligned} \frac{d}{dt} \mathcal{E}(\mathbf{X}_e(t)) &= \text{tr} \left\{ (\mathbf{X}(t) - \hat{\mathbf{X}})^T \frac{d}{dt} \mathbf{X}(t) \right\} \\ &= -\text{tr} \left\{ (\mathbf{X}(t) - \hat{\mathbf{X}})^T g(\mathbf{X}(t)) \right\}. \end{aligned}$$

As a result, $\frac{d}{dt} \mathcal{E}(\mathbf{X}_e) = -\text{tr} \left\{ \mathbf{X}_e^T h(\mathbf{X}_e^T, \hat{\mathbf{X}}) \right\} + o(\|\mathbf{X}_e\|_F^2)$.

Using (24) – (25) and the fact that $\mathbf{H} = \hat{\mathbf{U}}\hat{\mathbf{V}}^T$, it can be shown that

$$\begin{aligned} \frac{1}{2} \text{tr} \left\{ \mathbf{X}_e^T h(\mathbf{X}_e, \mathbf{X}) \right\} &= \text{tr} \left\{ \mathbf{U}_e^T (\mathbf{W} \odot (\mathbf{U}_e \mathbf{V}^T)) \mathbf{V} \right. \\ &\quad \left. + \mathbf{V}_e^T (\mathbf{W}^T \odot (\mathbf{V}_e \mathbf{U}^T)) \mathbf{U} \right\} \\ &\quad + \text{tr} \left\{ \mathbf{U}_e^T (\mathbf{W} \odot (\mathbf{U} \mathbf{V}_e^T)) \mathbf{V} \right\} \\ &\quad + \text{tr} \left\{ \mathbf{V}_e^T (\mathbf{W}^T \odot (\mathbf{V} \mathbf{U}_e^T)) \mathbf{U} \right\}. \end{aligned}$$

Note that under $\mathbf{H} = \mathbf{H}$, we have $\mathbf{W} = \mathbf{1}_{N \times N}$. In addition, if $\|\mathbf{V}_e\|_F = o(\|\mathbf{U}_e\|_F)$, i.e., $\|\mathbf{V}_e\|_F \ll \|\mathbf{U}_e\|_F$, then

$$\begin{aligned} \frac{1}{2} \text{tr} \left\{ \mathbf{X}_e^T h(\mathbf{X}_e, \mathbf{X}) \right\} &= \text{tr} \left\{ \mathbf{U}_e^T \mathbf{U}_e \mathbf{V}^T \mathbf{V} \right\} + o(\|\mathbf{U}_e\|_F^2) \\ &= \text{tr} \left\{ \mathbf{U}_e \mathbf{V}^T \mathbf{V} \mathbf{U}_e \right\} + o(\|\mathbf{U}_e\|_F^2) \\ &= \sum_{j=1}^N \mathbf{u}_j^{(e)} \mathbf{V}^T \mathbf{V} \mathbf{u}_j^{(e)T} + o(\|\mathbf{U}_e\|_F^2) \\ &\geq \sum_{j=1}^N \lambda_K(\mathbf{V}^T \mathbf{V}) \|\mathbf{u}_j^{(e)}\|^2 + o(\|\mathbf{U}_e\|_F^2) \end{aligned}$$

where $\mathbf{u}_j^{(e)}$ is the j th row vector of the matrix \mathbf{U}_e . As a result, we have

$$\frac{d}{dt} \mathcal{E}(\mathbf{X}_e) \leq -2\lambda_K(\hat{\mathbf{V}}\hat{\mathbf{V}}^T) \|\mathbf{U}_e\|_F^2 + o(\|\mathbf{U}_e\|_F^2)$$

proving (27).

If $\|\mathbf{U}_e\|_F = o(\|\mathbf{V}_e\|_F)$, the derivation to show (28) is similar.

REFERENCES

- [1] A. Beck, P. Stoica, and J. Li, "Exact and approximate solutions of source localization problems," *IEEE Trans. Signal Process.*, vol. 56, no. 5, pp. 1770–1778, 2008.
- [2] H.-D. Qi, N. Xiu, and X. Yuan, "A lagrangian dual approach to the single-source localization problem," *IEEE Trans. Signal Process.*, vol. 61, no. 15, pp. 3815–3826, 2013.
- [3] X. Sheng and Y.-H. Hu, "Maximum likelihood multiple-source localization using acoustic energy measurements with wireless sensor networks," *IEEE Trans. Signal Process.*, vol. 53, no. 1, pp. 44–53, 2005.
- [4] C. Meesookho, U. Mitra, and S. Narayanan, "On energy-based acoustic source localization for sensor networks," *IEEE Trans. Signal Process.*, vol. 56, no. 1, pp. 365–377, 2008.
- [5] Y. Liu, Y. H. Hu, and Q. Pan, "Distributed, robust acoustic source localization in a wireless sensor network," *IEEE Trans. Signal Process.*, vol. 60, no. 8, pp. 4350–4359, 2012.
- [6] C. Liu, Y. V. Zakharov, and T. Chen, "Broadband underwater localization of multiple sources using basis pursuit de-noising," *IEEE Trans. Signal Process.*, vol. 60, no. 4, pp. 1708–1717, 2012.
- [7] H. Chen, Q. Shi, R. Tan, H. V. Poor, and K. Sezaki, "Mobile element assisted cooperative localization for wireless sensor networks with obstacles," *IEEE Trans. Wireless Commun.*, vol. 9, no. 3, 2010.
- [8] T. He, C. Huang, B. M. Blum, J. A. Stankovic, and T. Abdelzaher, "Range-free localization schemes for large scale sensor networks," in *Proc. Int. Conf. Mobile Computing and Networking*, 2003, pp. 81–95.
- [9] J. Blumenthal, R. Grossmann, F. Golatowski, and D. Timmermann, "Weighted centroid localization in Zigbee-based sensor networks," in *Prof. IEEE Int. Symp. Intelligent Signal Process.*, 2007, pp. 1–6.
- [10] J. Wang, P. Urriza, Y. Han, and D. Cabric, "Weighted centroid localization algorithm: theoretical analysis and distributed implementation," *IEEE Trans. Wireless Commun.*, vol. 10, no. 10, pp. 3403–3413, 2011.
- [11] S. Choudhary and U. Mitra, "Analysis of target detection via matrix completion," in *Proc. IEEE Int. Conf. Acoustics, Speech, and Signal Processing*, 2015, pp. 3771–3775.
- [12] J. Chen and U. Mitra, "Rotated eigenstructure analysis for source localization without energy-decay models," in *Proc. Int. Conf. Digital Signal Process.*, London, UK, Aug. 2017.
- [13] R. Lefort, G. Real, and A. Dr meau, "Direct regressions for underwater acoustic source localization in fluctuating oceans," *Applied Acoustics*, vol. 116, pp. 303–310, 2017.
- [14] Y. Jin, W.-S. Soh, and W.-C. Wong, "Indoor localization with channel impulse response based fingerprint and nonparametric regression," *IEEE Trans. Wireless Commun.*, vol. 9, no. 3, pp. 1120–1127, 2010.
- [15] W. Kim, J. Park, J. Yoo, H. J. Kim, and C. G. Park, "Target localization using ensemble support vector regression in wireless sensor networks," *IEEE Trans. on Cybernetics*, vol. 43, no. 4, pp. 1189–1198, 2013.
- [16] S. Choudhary, N. Kumar, S. Narayanan, and U. Mitra, "Active target localization using low-rank matrix completion and unimodal regression," *arXiv preprint arXiv:1601.07254*, 2016.
- [17] J. Chen and U. Mitra, "Underwater acoustic source localization using unimodal-constrained matrix factorization," in *Proc. Asilomar Conf. Signals, Systems and Computers*, Pacific Grove, CA, USA, Nov. 2017.
- [18] E. Candes and B. Recht, "Exact matrix completion via convex optimization," *Commun. of the ACM*, vol. 55, no. 6, pp. 111–119, 2012.
- [19] E. J. Candes and Y. Plan, "Matrix completion with noise," *Proceedings of the IEEE*, vol. 98, no. 6, pp. 925–936, 2010.
- [20] A. N meth and S. N meth, "How to project onto an isotone projection cone," *Linear Algebra and its Applications*, vol. 433, no. 1, pp. 41–51, 2010.
- [21] C. R. Berger, S. Zhou, J. C. Preisig, and P. Willett, "Sparse channel estimation for multicarrier underwater acoustic communication: From subspace methods to compressed sensing," *IEEE Trans. Signal Process.*, vol. 58, no. 3, pp. 1708–1721, 2010.
- [22] S. Beygi and U. Mitra, "Multi-scale multi-lag channel estimation using low rank approximation for OFDM," *IEEE Trans. Signal Process.*, vol. 63, no. 18, pp. 4744–4755, 2015.
- [23] L. M. Brekhovskikh, *Fundamentals of ocean acoustics*. Springer Science & Business Media, 2003.
- [24] M. Kaul, B. Yang, and C. S. Jensen, "Building accurate 3D spatial networks to enable next generation intelligent transportation systems," in *Proc. IEEE Int. Conf. Mobile Data Management*, 2013, pp. 137–146.
- [25] V. Vu, "Singular vectors under random perturbation," *Random Structures & Algorithms*, vol. 39, no. 4, pp. 526–538, 2011.
- [26] M. Rudelson and R. Vershynin, "Non-asymptotic theory of random matrices: extreme singular values," *arXiv preprint arXiv:1003.2990*, 2010.